UNIVERSITY
OF TRENTO - Italy
DEPARTMENT OF INDUSTRIAL ENGINEERING

XXIX cycle

Doctoral School in Materials, Mechatronics
and Systems Engineering

Planar copper containing anode-supported solid oxide fuel cells

Vincenzo De Marco

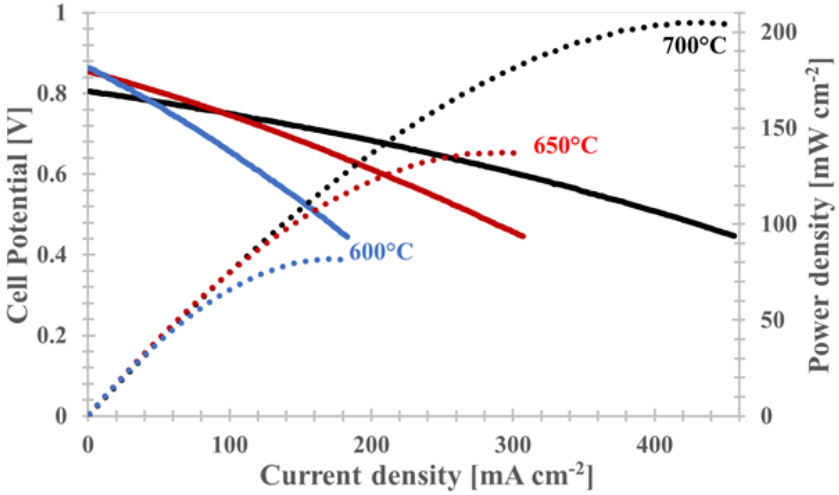

Month 2017

PLANAR COPPER CONTAINING ANODE-SUPPORTED SOLID OXIDE FUEL CELLS

Vincenzo De Marco

E-mail: vincenzo.demarco@unitn.it

Approved by:

Prof. - - - - - - - - -, Advisor
Department of - - - - - - - - -
University of - - - - - - - - -, Country.

Prof. - - - - - - - - -,
Department of - - - - - - - - -
University of - - - - - - - - -, Country.

Ph.D. Commission:

Prof. - - - - - - - - -,
Department of - - - - - - - - -
University of - - - - - - - - -, Country.

Prof. - - - - - - - - -,
Department of - - - - - - - - -
University of - - - - - - - - -, Country.

Prof. - - - - - - - - -,
Department of - - - - - - - - -
University of - - - - - - - - -, Country.

University of Trento,

Department of Industrial Engineering

Moth 2017

University of Trento - Department of Industrial Engineering

Doctoral Thesis

Vincenzo De Marco - 2017
Published in Trento (Italy) – by University of Trento

ISBN: - - - - - - - - -

Abstract

Planar copper-containing anode supported Intermediate Temperature Solid Oxide Fuel Cells (IT-SOFCs) were produced by single step cosintering. The anode and the electrolyte were realized through water-based tape casting, the cathode being added by screen printing. A 5 mol% of Lithium oxide addition allowed reducing the Gadolinia-Doped Ceria (GDC)-based electrolyte sintering temperature below the copper oxide melting point. IT-SOFCs sintered at 950°C revealed a power density peak of 26 mW cm^{-2} at 650°C in H_2, the maximum CuO amount within the anodic cermet being limited at 35 vol%. To improve the cell performance, the anode electrolyte thickness ratio was increased, in order to take advantage by the compressive tensile state induced by the supporting to the thinner layer, this leading to a further sintering temperature reduction and to avoid cracks due to the thermal expansion coefficient (TEC) mismatch existing between anode and electrolyte. IT-SOFCs at 900°C showed a power density peak of 200 mW cm^{-2} at 700°C in H_2. Electronic impedance spectroscopy pointed out anode performances comparable with those obtained by using conventional Ni-based cermet electrodes. In biogas, 45 vol% CuO containing SOFC achieved a power density peak of 38 mW cm^{-2} at 700°C.

Table of contents

Chapter I

Introduction

Solid oxide fuel Cells (SOFCs) are among the most promising devices for an environment-friendly energy conversion, due to reasons like their high fuel flexibility and to the possibility to be coupled within hybrid system for cogeneration purposes[1,2,3,4,5,6]. The aim to guarantee power also to small scale and domestic applications have recently lead the research towards lower operating temperature, within the "intermediate temperature" (IT) range (400-750°C), due to better stability and durability, lower corrosion rate and overall cost[7]. The principal approach that can allow to decrease IT-SOFC service temperatures without determining valuable performance reductions are fundamentally two: (1) decreasing the thickness of the electrolyte, thus reducing the specific ohmic resistance of the cell and (2) increasing the conductivity of the electrolyte at lower temperature. The material traditionally used in SOFC as electrolyte is yttria-stabilized zirconia (YSZ), due to its high mechanical and chemical stability and high ionic conductivity over a wide range of temperatures and oxygen partial pressures. Nevertheless, the conductivity of YSZ decreases in the IT range, this causing the necessity to find alternative materials. One of the preferred electrolyte materials for IT-SOFC is actually gadolinia doped-ceria (GDC), because of its higher ionic conductivity at lower temperature[10]. The poor densification behavior of GDC (in some cases achievable only above 1500°C[11]) is the main issue associated with its use. In the current approach, it is proposed to promote sintering at lower temperature by using sintering aids although this can determine variable effects on conductivity[12,13,14,15]. Another issue to be faced in SOFC is the anode poisoning due to carbon and/or sulphur impurities contained in hydrocarbon fuels[16]. At the state of the art, anodes are often made by YSZ and Ni, this latter being toxic and deactivated by contaminants present in available fuels even in parts per million levels[17-19]. Strong efforts have been made to develop innovative anode materials, like metal sulfides, cermets, ceria doped-oxides and perovskites. The literature review suggests, as an overall conclusion, that the use of innovative copper-based anode represents a potential solution to the specific inconvenient[20].

The fundamental aim of the present work was the realization of planar Ni-free IT-SOFC able to be fed with fuel different than pure hydrogen (like, for example, biogas and sulphur containing methane). For this reason, according to some previous works[20], copper was selected as the metal compound in the anodic GDC cermet. The cosintering of the GDC/copper-based supporting anode with the GDC electrolyte represented an additional important issue. Doping of GDC was investigated to accomplish the relatively low melting point of CuO but realizing gas-tight electrolyte.

The cell production is followed by the electrochemical characterization of the produced planar copper containing anode supported IT-SOFCs. To analyse such data and in

order to maximize the cell performances, the effect of different parameters have to be considered. In particular, the CuO concentration within the anodic cermet plays a fundamental role in the cell performance, due to the enhanced electronic conductivity provided by a copper increasing.

Unfortunately, thermal expansion coefficient (TEC) mismatch[20] during the cooling stage after sintering can induce the formation of cracks and even failures when an excessive CuO load is used in the anode. As a matter of fact, TEC mismatch is responsible for residual stresses in the SOFC-constituting layers. In addition, uneven sintering rate between anode and electrolyte can be responsible for differential densification of the two layers[21-24].

In order to eventually further reduce the electrolyte sintering temperature, one possible constructive strategy involves the development of compressive stresses in such layer upon co-sintering the multilayered cell. The difference of shrinkage rate (dε/(dt)) between anode and electrolyte can generate such desired residual stress.

Stresses generated upon sintering can be reduced by tailoring anode and electrolyte thickness and composition[23]. Stresses that arise upon sintering because of the different shrinkage rate between the layers can be responsible for flaws, delamination, retarded densification which are particularly undesirable in the electrolyte while, at least to some extent, they do not influence the anode performance, due to its necessary porous structure. In addition, mismatch stresses generated during the sintering period generally place the layer that have a more rapid densification rate in biaxial tension; therefore, the other layers are subjected to compressive stresses, which can help densificatio [25, 26]. On this basis, at a first approximation, in order to obtain an electrolyte with gas-tight microstructure, one possible constructive strategy could involve the development of compressive stresses in the electrolyte upon co-sintering. Although, the multilayered cell is non-symmetrical (the anode being always thicker than the electrolyte and the cathode and the constituting materials possessing different thermal and elastic properties, one can simplify the system, as it is subjected only to planar deformations upon sintering, i.e. neglecting any bending effect. In addition, also the effect of the cathode during sintering can be neglected because of its typical very limited thickness and high porosity. According to previous works[20, 25, 26] the equibiaxial stress generated by sintering mismatch in the electrolyte can be approximated as:

$$\sigma_{el} = \frac{1}{1+\frac{\alpha}{r}} \beta \, \Delta\varepsilon \qquad (1.1)$$

where *r* is the thickness ratio between the anode and the electrolyte, α a constant depending on the viscoelastic properties of the multilayer and β depending on the viscoelastic properties of the electrolyte, only, and $\Delta\varepsilon$ is the mismatch strain ($\Delta\varepsilon = \varepsilon_{el} - \varepsilon_{an}$), this being a function of temperature.

In the case of an asymmetric bilayer, like in a half-cell consisting of the anode and the electrolyte, a curvature is generally developed upon the sintering process due to mismatch in shrinkages and/or shrinkage rates and a more complicated stress field is generated[21-26]. Nevertheless, without entering in such details, according to if $\Delta\dot{\epsilon} < 0$ (i.e., the fastest shrinking layer is the anode), the electrolyte goes under compression with clear advantage to its densification; and in the SOFC configuration of interest here (with GDC electrolyte and CuO/GDC anode), the presence of larger CuO amount in the anode could definitely induce an anticipated sintering of this latter[20] with beneficial effects on the electrolyte. In addition, Eq. 1.1 points out also that the stress intensity within the electrolyte increase for smaller *r*, i.e. for increasing anode thickness.

As already mentioned, an additional source of residual stresses in a multi-layered system is the thermal expansion mismatch during cooling after sintering. In this case, the behaviour of the material can be considered simply elastic and stresses (calculated like in Eq. (1.1)) are generated in each layer due to thermal strain difference. For the SOFC composition considered in the present work, since CuO has a TEC larger than GDC ($\approx 13 \cdot 10^{-6}$ K^{-1} compared to $\approx 9.4 \cdot 10^{-6}$ K^{-1} [20]), larger amount of CuO in the anode implies more intense tensile stresses in the electrolyte, which can be detrimental for the integrity of this latter. Nevertheless, it is also clear that such stresses can be reduced if sintering is carried out (and possible) at lower temperature.

The basic idea to produce planar copper-based anode-supported IT-SOFC with improved performances is therefore to reduce the sintering temperature of GDC by using sintering aids and use thicker anode. In the present work, lithium oxide was used to reduce the sintering temperature of 10 mol% gadolinia doped-ceria used for realizing by tape casting the electrolyte and, with CuO addition, the anode. The behaviour of planar IT-SOFC where the anode thickness and CuO content were changed was investigated to point out possible beneficial combinations.

A key role is also played by the possible pore former addition in the anode tape casting recipe. In fact, a too densified electrode microstructure can negatively affect the Open Circuit Voltage (OCV) and, at the meantime, reduce the triple phase boundaries, where the electrochemical reaction takes place.

Chapter II

Background

2.1 Introduction

A Solid Oxide Fuel Cell (SOFC) is an energy conversion device able to convert the chemical energy of a fuel in to electrical energy. The conversion occurs like in a conventional battery, through electrochemical combination of the reactants. A SOFC does not discharge with time but continues generating electricity as long as fuel and oxidant are supplied to the electrodes, this constituting a difference with batteries.
In a SOFC, the chemical energy of the fuel is not converted in thermal energy by combustion. Due to this fact the SOFC efficiency does not obey to the Carnot cycle limitation. If we consider an ideally reversible heat engine, operating between the temperatures T_1 and T_2 ($T_1 < T_2$), the maximum efficiency is given by:

$$\eta = 1 - \frac{T_1}{T_2} \quad (2.1)$$

Thus, to increase the efficiency, the difference between T_1 and T_2 has to be as large as possible but, due to the limited stability of the materials, it is not possible to overtake operating temperatures allowing achieving efficiency higher than ≈ 30%.
Instead, a SOFC can get efficiency higher than any other known thermal device (>50%), and such efficiency can be further increased by coupling the SOFC with other devices (e.g.: micro turbine) able to convert the unutilized fuel in to thermal energy (combined heat and power systems). Others advantages of the SOFC is the absence of moving parts (this resulting in a limited operating noise) and the theoretical fuel flexibility. In this chapter, there is an introduction of the cell functioning principles and a discussion about the materials utilized and the problems generated by using fuel different from hydrogen. Finally, there is an overview of the most common configurations and architectures.

2.2 SOFC principles and thermodinamycs

In a SOFC, a solid electrolyte is put in the middle of two electrically conductive electrodes: the anode (or fuel electrode) and the cathode (or air electrode). They are connected through an external current collector (Fig. 2.1).

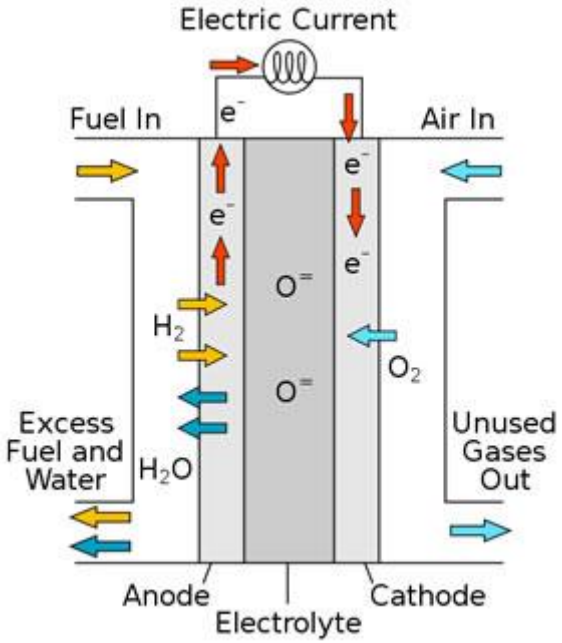

Figure II - 1. Schematic representation of the operating principle of the SOFC. Hydrogen is oxidized at the anode; oxygen is reduced at the cathode. The oxygen ions diffuse through the electrolyte to the anode side, where water is generated[27].

The most common fuel, thanks to its high reactivity, is the hydrogen. The fuel cell reaction can be divided in to two electrochemical half-cells reactions. At the cathode, the oxygen is reduced through the reaction:

$$4O_{2_c} + 4e^- = 2O^{2-}{}_e \quad (2.2)$$

The inverse reaction occurs at the anode:

$$2O^{2-}{}_e = 4O_{2_a} + 4e^- \quad (2.3)$$

Thus, the overall reaction results to be

$$O_{2_c} = O_{2_a} \quad (2.4)$$

In the previous equations, the subscripts c, a and e stand for the states at the anode, the cathode and the electrolyte.

In a preliminary stage, a SOFC can be considered as a concentration cell, where the partial pressure of oxygen on both sides defines the reversible thermodynamic voltage E_r, described by the Nernst equation

$$E_r = \frac{RT}{4F} ln \frac{P_{O_2 c}}{P_{O_2 a}} \ (2.5)$$

In the previous equation, R is the gas constant (=8314 J/mol·K), T the temperature expressed in Kelvin, F is the Faraday constant (=9648·10^4 C/mol) and PO_2 is the oxygen partial pressure at the anode (a) and at the cathode (c). At the anode side, the oxygen partial pressure depends on the employed fuel and on its type and composition. If we consider the hydrogen, the anode reaction is:

$$H_{2a} + \frac{1}{2} O_{2a} = H_2 O_a \ (2.6)$$

The equilibrium constant K of the reaction can be expressed as:

$$K = \frac{P_{H_2 O_a}}{P_{H_2 a} \cdot P_{O_2 a}^{\frac{1}{2}}} \ (2.7)$$

We can calculate the oxygen partial pressure at the anode as:

$$P_{O_2 a} = (\frac{P_{H_2 O_a}}{P_{H_2 a} \cdot K})^2 \ (2.8)$$

Therefore, the Nernst equation becomes

$$E_r = E^0 + \frac{RT}{4F} ln P_{O_2 c} + \frac{RT}{4F} ln \frac{P_{H_2 a}}{P_{H_2 O_a}} \ (2.9)$$

In the previous equation

$$E^0 = \frac{RT}{2F} ln \ K \ (2.10)$$

is the reversible voltage when the partial pressure of the reactants are equal to unity (the standard state). Such voltage is related to the standard Gibbs free energy change of the reaction by the equation:

$$\Delta G = -nFE \ (2.11)$$

where n is the number of moles of oxygen required to oxidize the fuel. In the standard state, the equation becomes:

$$\Delta G^0 = -nFE^0 \quad (2.12)$$

The standard Gibbs free energy gives us information about the spontaneity of the reaction. It is defined through the standard enthalpy change ΔH^0 and the standard entropy change ΔS^0:

$$E^0 = -\frac{\Delta G^0}{nF} = -\frac{\Delta H^0 - T\Delta S^0}{nF} \quad (2.13)$$

ΔG^0 is the maximum electrical work output that can be obtained from (2.6), ΔH^0 is the total thermal energy available by the same reaction at constant pressure and $T\Delta S^0$ is the heat released or absorbed. Thus, it is possible to define the ideal thermodynamic efficiency as:

$$\varepsilon_T = \frac{\Delta G^0}{\Delta H^0} \quad (2.14)$$

Table 2.1 reports some thermodynamic function of the most common reaction in a SOFC. It has to be noted that for carbon and methane oxidation, the thermodynamic efficiency is almost 1.

The effect of temperature and pressure on the reversible voltage is shown by differentiating the Eq. 2.11 for a non-standard state:

$$\frac{\partial \varepsilon}{\partial T}_P = \frac{\Delta S}{nF} \quad (2.15)$$

$$\frac{\partial \varepsilon}{\partial P}_T = \frac{\Delta V}{nF} \quad (2.16)$$

In the previous equation ΔV is the change in volume. If hydrogen and carbon monoxide are considered, ΔS<0, which means that at increase in temperature correspond to a decrease in E_r. Conversely, for the direct methane oxidation, $\Delta G \approx \Delta H$, this making the reversible voltage independent of temperature and pressure.

Table II – 1. Standard free energy and enthalpy change, Nernst potential and thermodynamic efficiency for some common reaction in a SOFC[28]

Reaction	T [K]	ΔG^0 [kJ]	ΔH^0 [kJ]	E^0 [V]	ε_T
$H_2 + \frac{1}{2}O_2 = H_2O$	1000	-192.5	-247.3	0.997	0.78
	1250	-178.2	-249.8	0.924	0.71
$CO + \frac{1}{2}O_2 = CO_2$	1000	-195.4	-283.3	1.013	0.69
	1250	-173.2	-283.3	0.898	0.61
$CH_4 + 2O_2 = CO_2 + H_2O$	1000	-802.5	-800.4	1.039	1
	1250	-802.9	-801.2	1.039	1
$C + O_2 = CO_2$	1000	-396.6	-396.2	1.027	1
	1250	-396.6	-396.6	1.027	1

The potential provided by eq. 2.9 is the voltage between anode and cathode when no current is flowing. Such value is called Open Circuit Voltage (OCV) and is function of temperature, the type of the fuel and reactions and the partial pressure of the reactants and products. By comparing the theoretical value of OCV and the operating it is possible to verify that the partial pressure gradient between the two electrodes is kept and there is no gas leakage through the electrolyte. When the electrodes are connected through a load and there is the electrons flow along the circuit, there is a

voltage drops due to different irreversible effects. Such effects contribute to decrease the overall SOFC efficiency, which becomes:

$$\varepsilon_{FC} = \varepsilon_T \varepsilon_V \varepsilon_J \varepsilon_H \ (2.17)$$

In the previous equations, subscripts T, V, J and H stand for the thermodynamic, voltage, current and heating value efficiency, respectively. The voltage efficiency ε_V is defined as the ratio of the operating cell voltage under load to the reversible voltage:

$$\varepsilon_V = \frac{E}{E_r} \ (2.18)$$

The loss of voltage E depends on current density and it is called polarization η:

$$E = E_r - \eta \ (2.19)$$

Different effects contribute to give the total polarization: the activation polarization η_A, the concentration polarization η_D and the ohmic polarization η_Ω:

$$\eta = \eta_A + \eta_D + \eta_\Omega \ (2.20)$$

The overpotential can be optimized by properly choosing the materials, the cell design and the operating temperature and pressure.
The activation polarization η_A is function of the activation energy that has to be overcome by the reagents to react. For electrochemical reactions having η_A>50 mV, it is obtained by the Tafel equation:

$$\eta_A = a \pm b \log j \ (2.21)$$

where j is the current density, while a and b are constants related to the material, the catalytic activity and the type of the electrode reaction. Normally, the high operating temperatures of SOFC make the activation polarization smaller.
The insufficient velocity of reacting and reacted species to and away from the reaction sites as more current is drawn from the cell is the reason of concentration polarization η_D. When large currents are drawn from the cell, there is an increasing in the reactions velocity and the reacting species begin to be depleted in one or both of the electrodes. When the limiting reaction step is dominated by the diffusion of the species to and away from the electrodes, a limiting current j_L is reached. Such limit is function of the diffusion coefficient D, the activity of the reacting ions a_M and the thickness of the diffusion layer ∂ and it can be calculated through the Fick's law:

$$j_L = \frac{nFDa_M}{\partial} \quad (2.22)$$

and the concentration polarization can be expressed by:

$$\eta_D = \frac{RT}{nF} \ln\left(1 - \frac{j}{j_L}\right) (2.23)$$

This contribution becomes important when the current density j tends to j_L. Such value strongly depends also on the ease of access to the reacting sites of the electrodes. Therefore, this parameter is affected also by electrodes thickness, porosity, pore size and morphology.
The resistance of the cell for both ionic conduction through the electrolyte and the electronic conduction in the electrodes and the current collector are the reasons why ohmic polarization occurs, that we express through the Ohm's law:

$$\eta_\Omega = j\, R_{tot} \quad (2.24)$$

R_{tot} is the total resistance of the cell, which mostly depends on the ionic conductivity of the electrolyte. Thus, the ohmic resistance can be decreased by properly choosing the electrolyte materials, as well as the operating temperature.
The ratio between the actual current withdrawn and the current available from the complete conversion of the fuel gives us the current efficiency ε_J. When some of the fuel is not consumed, the current density j can be expressed through the Faraday's law:

$$j = nF\left(\frac{df}{dt}\right)_{consumed} \quad (2.25)$$

Where df/dt is the molar flow rate of the fuel. The current efficiency is given by:

$$\varepsilon_J = \frac{j}{j_F} \quad (2.26)$$

In the previous equation j_F is the current density available from the complete fuel oxidation.
Regarding the heating value efficiency ε_H, it can be considered when the fuel is not pure but it contains some electrochemically inactive species and it can be expressed as the ratio of the amount of heat of fuel species available to produce electricity to the total amount of heat energy contained in all the combustible species in the fuel gas.
The tipical current-voltage plot of an operating fuel cell is shown in Fig. II – 2.

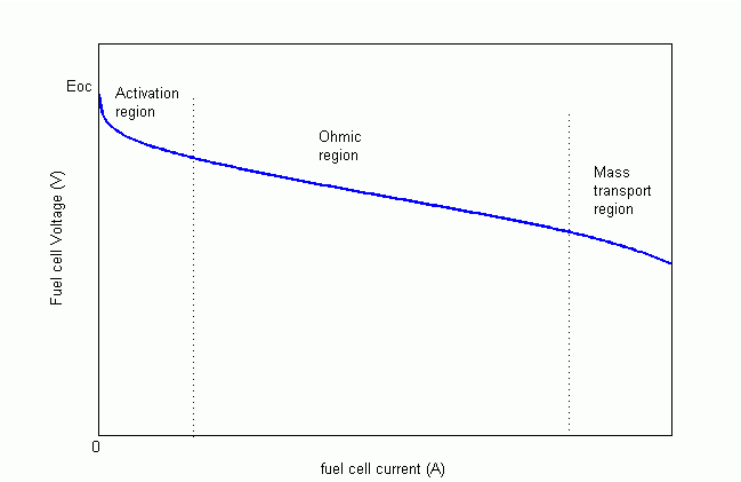

Figure II - 2. Typical current-voltage plot of a SOFC. The different polarization contribution to the voltage drop are indicated[32].

At low current densities values, the activation polarization mostly contributes to the voltage drop. By increasing the current density, the voltage drops linearly, this impling that the ohmic losses are predominant in this range. At high current values, mass transport effects become important and the rapid voltage drop observed is attributed to the concentration polarization.

The product between the operating voltage E and the current I allows to calculate the power output P_W:

$$P_W = E\ I \quad (2.27)$$

If we consider the effect of the overpotential on the operating voltage, the plot of the power output may be represented as in Fig. II – 3.

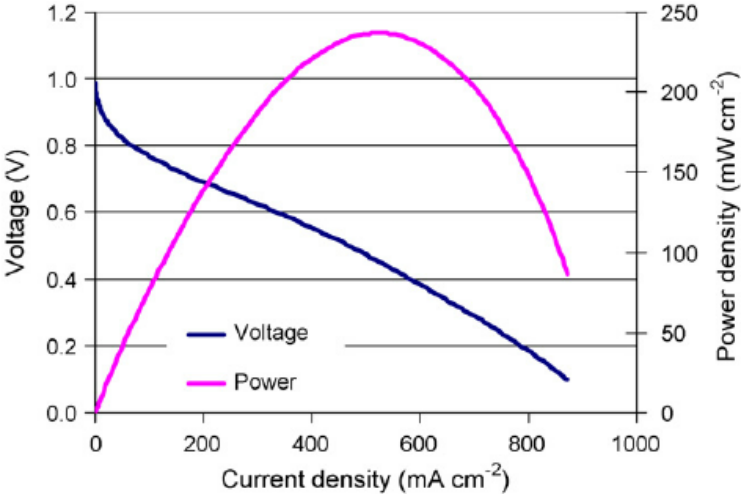

Figure II - 3. Typical power- current plot of an operating SOFC.

For extreme values of current, the power drops to zero and it has a maximum in between. In first approximation, the main contribution to the overpotential is ohmic, the relationship between voltage and current density is nearly linear. It can be written as:

$$E = E_r - E_\Omega = E_r - R_t I \quad (2.28)$$

Thus, we can define a parabolic expression for the power, expressed by:

$$P_W = IE_r - I^2 R_t \quad (2.29)$$

By differentiating Eq. 2.29 with respect to the current to zero, it is possible to calculate the value of current relative to the maximum power:

$$\frac{dP_W}{dI} = 0 \quad (2.30)$$

$$I_{P_{max}} = \frac{E_r}{2R_t} \quad (2.31)$$

Substitung the current from Eq. 2.31 in Eq. 2.28 gives the chance to get the operating voltage relative to the maximum power output:

$$E_{P_{max}} = \frac{E_r}{2} \quad (2.32)$$

Thus, to achieve the maximum power, the cell voltage is operating at 50% of the reversible voltage and in this case the voltage efficiency is ≈50%. Thus, the SOFC can operate in different regimes, depending on what is suitable for a certain type of application. If we operate at low current densities the efficiency is higher but with low power densities, more usable for stationary applications. For high current densities operating cells, higher power can be achieved, but with lower efficiency. Such devices are more indicated for mobile applications.

2.3 Materials and cell components

A SOFC is made by a series of solid layers with the electrolyte sandwiched between two porous electrodes. The materials selected for being used in the SOFC have several constrains due to more than just their specific role. Some parameters to be considered are: operating temperature, the architecture, the fabrication method, ionic and electronic conductivity of the materials, the porosity, resistance to high temperature, as well as the relative mechanical and chemical compatibility among the materials. The SOFC layers, in fact, require a high temperature treatment to achieve dense electrolyte layer to avoid gas leakage between the electrodes and to minimize the contribution of the ionic resistance. More cell components may be subjected to the heat treatment of the electrolyte, which normally requires the highest temperature and longest sintering cycle, depending on the fabrication procedure selected and on the cell configuration. Thus, the materials employed have to be stable and compatible in both heating and cooling stage of sintering, when it is possible the onset of large residual stresses fractures and debonding, that have to be avoided. General requirements of cell components and materials of interests are reviewed in the following sections.

2.3.1 Electrolyte

The most important characteristic of the electrolyte layer in a SOFC is its ability to conduct exclusively the ions. The ionic conduction in solid electrolyte is primarly determined by the presence of lattice defects. These defects can be stoichiometric or not. Also the partial pressure P_{O_2} has considerable relevance: for values to those required to maintain stoichiometry, the oxide becomes metal-deficient with excess of interstitial defects. The negative charge is balanced by electron holes produced by the thermal activation of the electrons from the valence band to the conduction band. Thus, electron holes are the main charge carrier with a concentration usually increasing with P_{O_2} and the electrolyte loses functionality because the electrodes are short-circuited. In the case of lower oxygen partial pressure respect to stoichiometric condition, the oxide is rich in oxygen vacancies and free electrons are the main defects[29]. In general, for every condition of temperature and partial pressure, the ionic conductivity of pure solid oxide is too low for SOFC applications.

The most commonly material used as electrolyte for SOFC is YSZ. Fig. II – 4 shows the ionic conductivity versus temperature of fore some materials for high (II-4) and intermediate (II-5) temperature ranges.

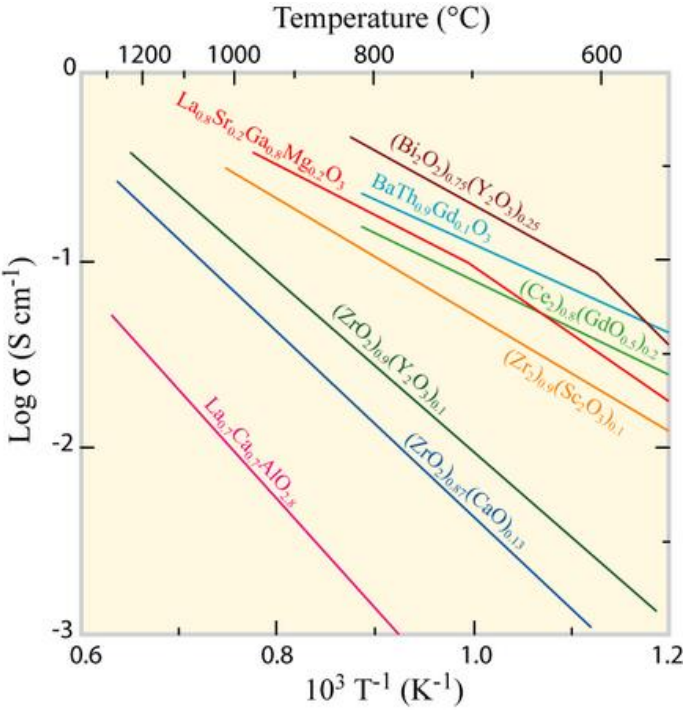

Figure II - 4. Conductivity of some ion conductors in intermediate temperature range[30]

Although YSZ is not the best ionic conductor, the others materials tipically have other issues to be faced like cost and difficulty in processing. At the present state YSZ is the state of the art electrolyte for high temperature SOFC application. However, the aim of our work being the production of IT-SOFCs, doped ceria is used and properly discussed in the next session.

2.3.1.1 Gadolinia-doped Ceria based electrolytes

One of the most diffused electrolytes in SOFC operating at intermediates temperatures is Gadolinia-doped Ceria (GDC)[31] . Ceria has a cubic fluorite structure and it is stable from the room temperature to the melting point without polymorphs.

Pure Ceria has a negligible electronic conductivity and free mobile oxygen vacancies are introduced by substituting Ce^{4+} with divalent or trivalent atoms such as La^{3+}, Y^{3+}, Gd^{3+}, Ca^{2+} and Sr^{2+}. If we fix the doping concentration, the ionic conductivity of doped ceria increases with increasing the dopant radius, up to a maximum correspondent to Gd^{3+}, before decreasing with further increasing of ionic radius[32]. Also the dopant concentration influences the conductivity that has a maximum for a specific concentration for every doping atom. When the concentration is further increased, the conductivity decreases, due to the attractive interactions between immobile doping ions and mobile oxygen vacancies[33]. The licterature suggests that Gd_2O_3 is the dopant exhibiting the highest conductivity[34, 35]. However, in doped CeO_2, the Ce^{4+} ion tends to reduce to Ce^{3+} at low oxygen partial pressure condition, this been offset by the creation of negative charge[36]. This phenomenon leads to electronic conductivity short-circuiting the cell, reducing the open circuit voltage (OCV) and its efficiency[37]. Another problem that has to be faced, related to the reduction of doped ceria at the anode side, is the lattice expansion resulting that can induce the formations of micro cracks and mechanical failure of the electrolyte[8].

The most problematic aspect regarding the employment of doped-ceria as electrolyte is represented by the high temperature required to get a full dense microstructure[9]. In fact, sintering temperatures higher than 1400°C are necessary and this could preclude any possibility to co-sinter doped ceria with other cell components because of instability or reactivity. In general, the sinterability of doped ceria is enhanced by decreasing the particle size or by the addition of transition metals[38].

2.3.2 Anode

The anode is where the electro-oxidation reactions of the fuel take place. The most important requirements are a good catalytic activity for those reactions, resistance to strong reducing environment, a sufficient porosity to ease the gas transport to and away from the reaction sites and a high electronic conductivity to ease the movement of electrons to the current collector. The anode is generally a cermet, which means a composite of ionically conductor ceramic material and a metal. The metal is tipically introduced in the oxidized form to be more resistant to high temperature oxidation and it is reduced to the metallic form before operation, in order to provide the electronic conductivity to the layer. The sites where the ionic and electronic conductors meet with the open porosity are where the reactions take place and it is called triple phase boundaries (TPB). A good distribution and contact of the three phases corresponds to a higher TPB, to a reduction of the overpotential and in an improvement of the performances. The most commonly used cermet material is Ni-YSZ due to the catalytic properties of Nickel toward hydrogen oxidation. However,

actually strong efforts are being produced to adapt the SOFC to be fed with hydrocarbons, thus other compositions have been proposed.

2.3.2.1 Issues related to the employment of C-based fuels

Although actual Ni-YSZ anodes show good performance and long-term stability for hydrogen, this changes when carbon-containing fuels feed the SOFC. As one can observe in Table II – 2, hydrogen has the highest energy density per mass than any other fuels but, due to the diffulties in storaging and distributing it, serious issues against the real implementation of a hydrogen-based energy economy have to be faced.

Table II – 2. Comparison of some energetic properties of hydrogen and methane.

	H_2	CH_4
Energy density [kWh/kg]	33.3	13.9
Density [g/l]	0.09	0.718
Energy density [kWh/l	0.5-2.4	2.6-3.4
Explosion range [vol%]	4-72.5	5-13.5

Moreover, water is the only by-product but hydrogen is not available in nature as single molecule but it is always bonded to another atom. It has to be produced by water electrolysis, or by steam reforming and partial oxidation of naptha and natural gas. Using natural gas, methane and other simple hydrocarbons directly in a SOFC, by direct oxidation or internal steam reforming they could constitute a valid alternative. When a molecule like methane is used to fuel a SOFC, the simple reaction of hydrogen oxidation is replaced with a more complex set of reactions. The direct oxidation of methane is one of the possible reactions:

$$CH_4 + 4O^{2-} = CO_2 + 2H_2O + 6e^- \quad (2.33)$$

However, this reaction is unlikely to directly occur, even in a case of a simple hydrocarbon such as methane. Instead, it is more probable to proceed as:

$$CH_4 + O^{2-} = CH_3OH + 2e^- \quad (2.34)$$
$$CH_3OH + 2O^{2-} = HCOOH + H_2O + 64 \quad (2.35)$$
$$HCOOH + O^{2-} = CO_2 + H_2O + 2e^- \quad (2.36)$$

Other possible reaction are methane cracking, which are followed by electrochemical reactions of the cracking products:

$$CH_4 = C + 2H_2 \quad (2.37)$$

$$C + 2O^{2-} = CO_2 + 4e^- \ (2.38)$$
$$H_2 + O^{2-} = H_2O + 2e^- \ (2.39)$$

It is also possible that there is only a partial oxidation: If this happens, the reaction produce a mixture of CO and H_2, called syngas, and produces electrons:

$$CH_4 + O^{2-} = CO + H_2 + 2e^- \ (2.40)$$

The production of carbon monoxide can lead to the Bouduard equilibrium reaction or to its electrochemical reaction:

$$2CO = C + CO_2 \ (2.41)$$
$$CO + O^{2-} = CO_2 + 2e^- \ (2.42)$$

In principle, the reaction above can take place by fuelling the cell only with dry methane, with no steam added. Carbon can be formed in both gas phase or as a solid deposit on anodic surface. The formation of C is very important, especially when it is in the form of solid coke. Regardless the coke formation process, this can cause the anode deactivation.
The most used strategy to solve this problem is the use of alternative anode materials that do not catalyse carbon formation. If we consider that the fuel is methane with steam, the immediate option would be the partial or complete substitution of nickel with another good reforming metal catalyst. Even if the use of an electronic conductor, like copper, decreases the catalyst content, the stability period results to be slightly increased[39]. Moreover, copper shows one of the highest conductivity values among metals ($5.96 \cdot 10^5$ $S \cdot cm^{-1}$), is inert toward C-H bond cleavage and carbon deposition and, compared to the other metals, is also cheap. On the other hand, the copper has a very low melting point (1083 °C), as well as its oxides. Copper forms two oxides: cuprite (Cu_2O) and tenorite (CuO). Tenorite is the stable oxide in the standard condition but it reduces to cuprite above 1026°C and melts above 1100°C. Cuprite is instable in air and it tends to form a CuO layer in humid conditions[40].

The melting temperatures constitute a big issue for both fabrication and operation. Firstly, the operating temperatures required would be very close to the Cu melting point. This implies that, for a Cu-based anode SOFC, the selection of the electrolyte must to be oriented toward better ionic conductors in intermediate temperature range (500-600 °C). As second, the commonly used procedure of high sintering temperature of the composite cermet with the copper oxide cannot be easily applied in this case. Generally, the used oxides are formed and heated up to a temperature sufficient to sinter ceramic and create a mechanically stable and well-connected structure. For this treatment temperatures higher than CuO and Cu_2O melting point are required. To

solve this problem, the solution applied in this work is the use electrolyte sintering aid able to get a fully dense microstructure at temperature lower than copper oxide melting point.

2.3.3 Cathode

The cathode is where the electrochemical reduction of oxygen occurs. Thus, in order to properly work, the cathode material must have several roles such as reduction of molecular oxygen, transport of ions to the electrolyte interface and distribution of the electrical current associated with the oxygen reduction reaction. Moreover, in addition to both the catalytic activity and the electrical conductivity, the material used in the cathode must be stable in strongly oxidising atmosphere and have both chemical and mechanical compatibility with other cell components. The majority of the materials used for the fabrication of this electrode have perovskite structure. For high-temperature operating cells, the state-of-the-art cathode is a mixture of lanthanum strontium manganite (LSM) and YSZ. Other cathode materials, more suitable for intermediate operating temperature, are Lantanum strontium cobaltite (LSC) and lanthanum strontium/cobalt ferrite (LSCF). These latter are mixed electronic ionic conductors (MIEC) and can be employed as single-phase cathode. A mixed conductor has the benefit to extend the area of reaction of the whole electrode surface area, resulting in a lower cathode polarization resistance. The formation of cracks and the delamination can be avoided by properly adding the electrolyte material, so that a better match of TEC. Normally, cobalt based perovskites show higher ionic and electronic conductivity than any other cathode material. Such cathode are characterized by an high value of TEC (higher than $20 \cdot 10^{-6}\ °C^{-1}$), than can be reduced by substituting some Co with Fe. The thermal expansion coefficient LSCF matches with GDC and the cathode does not show any degradation sign after 500h of operation[35].This suggest this solution as very promising cathode for IT-SOFCs.

2.4 Motivation of the work

Based on the above mentioned background, it is possible to state two main motivations related to our work: firstly, the fundamental aim is the realization of planar Ni-free IT-SOFC with which it is possible to use fuels different than pure hydrogen (e.g.: biogas and sulphur containing methane). Thus, according to some previous works[16, 20], our research moves towards the utilization of copper as the metal compound in the anodic GDC cermet. Unfortunately, GDC shows a very poor densification behavior (> 1400°C[11]), while the CuO has a relatively low melting point, this latter not exceeding 1050°C. Consequently, the cosintering of the GDC/copper-

based supporting anode with the GDC-based electrolyte represents an additional important issue. Thus, the second motivation is to find a processing strategy able to reduce the GDC sintering temperature at a temperature compatible with the melting point of the CuO, in order to achieve a one step cosintering of the whole IT-SOFC. In the current approach, it is proposed to promote sintering at lower temperature by using sintering aids[12,13,14,15]. In particular[20, 48], Li_2O seems to have a really favourable effect on the decreasing of the onset sintering temperature of GDC.

Chapter III

Materials and experimental procedures

In this chapter, an overview of the materials and the instruments utilized for the research development is reported.

3.1 Materials

In this section, all materials used to realize the tape, such as powder, solvent and all the organic additives are properly described and analysed.
The powder used for the electrolyte is Gadolinia-doped ceria with Gadolinia in a concentration equal to 10 mol%. With component percentages are:
- CeO_2 = 0.9 mol
- Gd_2O_3 = 0.1 mol

Values obtained according to $Ce_{1-x}Gd_xO_{2-x/2}$ formula, where x is the concentration of the dopant. Table III-1 shows the particle size of the powder indicated in the datasheet containing the specifications of the same, provided by Treibacher industrie.

Table III – 1. GDC powder specifications

d_{50}	0.27 µm
d_{90}	0.40 µm
SSA (Specific Surface Area)	9.1 m^2/g

The importance of the SSA resides in the fact that many parameters can be adjusted in relation to it. In the specific case the amount of dispersant was calculated considering the active part (PA), namely the mass of the solid part of the dispersant solution, in relation to the unit of specific surface area of the powder. Moreover, two different sintering aids were tested, bismuth oxide and lithium oxide. The starting doping powders were $Bi(NO_3)3{\cdot}5H_2O$ (Sigma Aldrich, ACS reagent, ≥98.0%, Product Number 383074) and $LiNO_3$ (Avantor Materials, Baker analyzed reagent, Product number 2384-01). For the anode, CuO powder (Sigma Aldrich, Product number 208841) was utilized. Solvent and various organic additives, necessary for both electrolyte and anode production, were employed and are below shown. As dispersant, Darvan 821-A was found as one of the best usable for GDC powders[42-44]. Such dispersant is constituted by a PAA solution (Poly Ammonium acrylate) in water and allows the deflocculation of the powders by electrostheric effect.Table III – 2 shows the specifications of this organic additive.

Table III – 2 Dispersant specifications

Darvan 821 – A	
pH	7-7.5
Solid load [wt%]	40
Density [g/cm^3]	1.16-1.19
Vicosity	15-50 cps

In the present work, water (in our case bi-distilled) was chosen as solvent. The Rohm and Haas Company produces the binders used in the lab. They are acrylic-based polymers with high molecular weight. They are provided as low viscosity emulsions. According to the glass transition temperature of the polymer, it will improve the strength and green density for a given ceramic process.
In the case of tape casting the products that best meet the process requirements are:
DURAMAX B -1000, used as a plasticizer for its low T_g
DURAMAX B -1014, it used as a binder for its high T_g
Table III – 3 shows the fundamental properties of the two additives.

Table III – 3. Binder and plasticizer specifications

Duramax code	T_g [°C]	pH	Solid load [wt%]	Dimension of particles (nm)	Viscosity (mPa·s)
B 1000	-26	9.6	55	370	140
B 1014	29	3	45	85-140	750

The cathode starting powder was LSCF (Treibacher Industrie, Lot. EA 14/11.2).

3.2 Experimental procedure

3.2.1 Slurry preparation

3.2.1.1 Mixing

The first step necessary for preparing a ceramic suspension is dispersing the powders in an optimal way. The dispersion mechanism provides that the ceramic powder particles are perfectly deflocculated in the aqueous suspension.
The mixing process was then realized by adding water, dispersant, powder and zirconia balls into a container, which is subsequently introduced into a suitable mixer, the vortex. The dispersion/deflocculation of a powder in a liquid takes place in three fundamental steps:

1.The surface of the powder particles is wetted by the solvent, after which the light agglomerates remain "stuck" between them because of the Van der Waals electrostatic forces;
2. The primary particles must be mechanically separated and this happens thanks to the action of the spheres of zirconia vortex; once finished this step, they are evenly distributed throughout the liquid
3. The state of perfect distribution of the particles in the solvent must be stabilized and protected. This latter action is made by the dispersant.

3.2.1.2 Deairing

The deairing process is necessary to remove the air stored within the suspension because of the mixing vortex. It is done by connecting a glass ampoule, where is previously stored the suspension immediately after the mixing step, to a venturi pump. The ampoule is suspended on a magnetic mixer, this expedient is of fundamental importance because the liquid under vacuum tends to create a dry film on its surface. The drying effect is due to the fast evaporation of water from the suspension surface caused by the vacuum in the bulb. To avoid this phenomenon, this method creates the minimum agitation sufficient to keep the free liquid surface dry. A second important trick is to not proceed with the de-aeration of the suspension until it reaches room temperature; in fact, the suspension, just extracted from the vortex, is very hot due to internal friction and impact shocks of powder particles and small spheres of zirconia. A deaeration made of a hot liquid leads to a very fast lowering of its temperature and accentuates the drying phenomenon, not desired in this phase. Slurry having a solid load between 16 and 30 vol% (2 vol% step) were tested. For suspensions with high SL (in the case of GDC close to 30 vol%), this phase becomes very critical since it covers any bubbles in the first seconds of the deaeration stage, leaving residues on the ampoule inner walls, which, once dried, fall in solid form in the liquid. The presence of a low viscosity slurry is a strong help in this process. To avoid the presence of solid phases after the deaeration a filtering is carried out before continuing with the next step. In our case we were used polymeric filters with mesh of 100 microns. For the above mentioned reasons, both for the deaeration process itself (with its partial drying of the slurry) and for the subsequent filtering, there is a loss in weight of the suspension compared to the initial quantity extracted after mixing. This leads compute the "deaeration efficiency", defined as the ratio between the post-deairing and the mass of the suspension after mixing vortex.

3.2.1.3 Additive mixing

The use of additives in tape casting is relatd to the need to have good mechanical properties in the green product. These materials, compounds of a solid

polymeric part diluted in water, allow the powder grain to remain cohesive and to maintain the desired shape at the same time, even after the green layer drying. The mixing of the additives was accomplished by pouring the suspension into an open container, then by immersing a Teflon impeller which is rotated at a constant number of RPM (in our case equal to 80 RPM) via a mixer Daihan scientific WiseStir HD-50D. The employed RPM were chosen after various tests. In fact, a too high speed can lead to resorption of air in the suspension, whereas a too low speed may not provide proper mixing even after a relatively long time.
The mixing process is the most critical since the used additives have pH different from each other. The pH of the GDC powder in water and dispersant (this latter being previously optimized through viscosimetric tests) was measured using a pH meter; the value amounts in a range of 7.5 - 8. By the addition of additives, which have a different starting pH, this value is altered.
If the pH decrease during the mixing process, the phenomenon of instability can arise; vice versa, if the ceramic suspension pH is kept at high values, the instability does not occur because the dispersant, beyond a certain maximum pH for which the ceramic powder particles are perfectly deflocculated, does not change its electrosteric function. The phenomenon of the instability results in a thickening of the slurry in a more or less evident way, depending on the variation of pH. Through various tests the minimum pH for which the agglomerate problem started to appear was determined

3.2.2 Tape casting process

The ceramic suspension film is produced by tape casting, using a device available in the laboratory. Before casting the suspension is further filtered to avoid the presence of any macroscopic agglomerate formed in the previous stage of mixing of the additives.
Doctor blade runs on a support material represented by a sheet of aluminum coated with polymeric materials (LDPE on a surface and on the other PET). Casting is realized on the LDPE side which facilitates the removal of the samples, once dried, due to its low wettability.
The obtained film is liquid, due to the high water content. The water is carefully removed, creating an atmosphere with constant humidity within the plexiglass case. The drying process is a critical phase, since the material tends to create cracks or to sag if it does not take place in an optimal way[45, 46].
In the case of GDC tape the humidity was kept at values of 80% for 15 min.

3.2.3 Analysis of viscosity

To carry out viscosimetric analysis, a rotational viscometer Myr mod was used. V2L, with a set of spindles (cylindrical rotating body to be immersed in the liquid) that allowed to measure the viscosity for a wide range of values (spindle September TL5 - TL7 , viscosity range from 1.5 to 6 · 105 mPas - cP) . The fluid was maintained at a constant temperature of 25°C, as described in ASTM - " Standard Test metods for Rheological Properties of Non - Newtonian Materials by Rotational viscosimeter " (D2196-10), through the use of a thermal bath (LAUDA C6). The viscosimetric analysis were performed on the suspension samples containing a fixed solid load (SL), i.e. the ratio between the volume of powder and the total volume, and by gradually varying the active part of the dispersant (AP), i.e. the mass of active part of dispersant for powder surface. In other words the mass of the solids that actively participates in the deflocculation of the powders in water.
The same type of tests was carried out at different SL value, progressively varying the AP, to check the progress of the viscosity as a function of both AP that of SL. The measurements were made by varying the AP from 0 mg/m^2 up to a PA of 1.25 mg/m^2 and the rotational speed between 3 and 200 rpm.

3.2.4 GDC doping and dilatometry

The starting doping compounds were $Bi(NO_3)3{\cdot}5H_2O$ and $LiNO_3$. GDC10 doping was accomplished by dissolving the nitrates in ethanol and adding the appropriate amount of GDC10. The dispersion was kept stirring on a hotplate at 90°C until complete evaporation of the ethanol. Bi-containing and Li-containing powders were calcined at 700°C and 650°C for 3 h, respectively. The powder was then ground and sieved (mesh size = 150 μm) to eliminate the largest agglomerates. Cylindrical samples (diameter = 13 mm, height = 4 mm) were formed by uniaxial pressing using 100 MPa maximum pressure. The sintering behavior of samples containing different dopant load were analyzed by dilatometry (Linseis L75 Platinum Series, Linseis Instrument) using an alumina support tube and constant heating rate of 10°C/m up to 1550°C in air flux. The Bi-containing samples were sintered in a furnace at constant heating rate of 10°C/m up to 1050°C with different holding time.

3.2.5 Production of IT-SOFC

The electrolyte was produced starting from water based slurry consisting of solvent (distilled water), dispersant and 5 mol% Li_2O-doped GDC powder. Such slurry

was kept in agitation for 2 h in a high-energy mixer and de-aired for 30 min. Hence, plasticizer and binder were added and the suspension was mixed for additional 20 min. The slurry was cast on a silicone-coated polyethylene terephthalate film in a laboratory scale tape caster, with a double blade apparatus (Mistler, Yardley, PA), by using a 200 μm blade height. The relative humidity in the tape casting chamber was kept constant at 80% to avoid the formation of cracks upon drying. The recipe used for the electrolyte production is shown in Table III-4. The 2 mol% Li_2O containing GDC powder was used for 25 vol% CuO-containing cells, while for all the other cells the 5 mol% Li_2O containing GDC powder was used.

A similar process was used for the production of the Cu-containing anode-supporting layer. A slurry consisting of different CuO powder amount (varying between 25 and 45 vol%), 2 mol% (for 25 vol% CuO containing cells) or 5 mol% Li_2O-doped GDC powder (65 vol%), distilled water and dispersant was produced; this was then de-aired after 2 h high-energy mixing. Plasticizer and binder were added and the suspension was tape cast (blade height = 250 μm), always controlling the relative humidity at 80%. Table III-5 shows the recipe followed for the production of the anode.

. Table III – 4 Composition of the suspension used for tape casting the electrolyte.

Material	Manufacturer/provider	Content (vol%)
2 or 5 mol% Li_2O-doped GDC10	Treibacher	17
Binder (Duramax B 1014)	Rohm and Haas	8
Plasticizer (Duramax B 1000)	Rohm and Haas	6
Dispersant (Darvan 821 A)	Vanderbilt Minerals	0.5
Distilled water		68.5

Table III – 5 Composition of the suspension used for tape casting the anode.

Material	Manufacturer/provider	Content (vol%)
5 mol% Li_2O-doped GDC	Treibacher	14.25-12.35-11.4-10.45
CuO	Sigma Aldrich	4.75-6.65-7.6-8.55
Binder (Duramax B 1014)	Rohm and Haas	12
Plasticizer (Duramax B 1000)	Rohm and Haas	6

Dispersant (Darvan 821 A)	Vanderbilt Minerals	2.5
Distilled water		60.5

To produce the anode-supported half cells, green disks (anode thickness ≈ 80 μm, electrolyte thickness ≈ 60 μm, diameter = 24-30 mm) were extracted by using a die cutter. The anodes disks and one electrolyte disk were stacked together and thermo-pressed at 80°C for 15 min under 30 MPa.

The cathode was produced mixing 50 wt% LSCF (Treibacher Industrie, Lot. EA 14/11.2) and 50 wt% GDC powder in ethanol (powder/solvent weight ratio = 1:1). The slurry was mixed for 2 h and terpineol (containing 4 wt% ethyl cellulose) was added in a 1:1 weight ratio with the powder. The slurry was then screen printed (diameter ≈ 20 mm) on the green half cell.

The green cells were sintered at 900°C or 950°C (heating rate = 1°C min^{-1}) in static air for 3 h. The cooling stage was controlled at 1°C min^{-1} down to 500°C, to limit the residual stresses due to the thermal expansion coefficient difference.

3.2.6 Electrochemical characterization

The anode reduction was performed in a controlled atmosphere, having a N_2 and an air flow rate of 141 ml min^{-1} and 471 ml min^{-1}, respectively. The hydrogen flux was kept at 20 ml min^{-1} for 1 h and it was increased up to 200 ml min^{-1} until the end of the reduction process. The electrochemical tests of 25 vol% CuO containing anode were carried out at 800°C and 700°C in a controlled atmosphere with a flux of 100 ml min^{-1} H_2 and 500 ml min^{-1} air, respectively. The more than 35 vol% CuO containing anode SOFCs were tested at temperatures between 550°C and 700°C in 200 ml min^{-1} H_2 and 471 ml min^{-1} air containing flux. Electrochemical measurements were performed by using Autolab PGSTAT302N potentiostat/galvanostat. EIS spectra were collected in the range of frequency 10 kHz e 0.01 Hz and using 10 mV perturbation amplitude. Electrochemical impedance spectroscopy parameters were evaluated at 600°C by using Zsimpwin 3.22 program.

3.2.7 Sintering temperature and anode composition analysis

After the electrochemical characterization, some cells were manually but carefully broken to expose a fracture surface orthogonal to the cell plane. The microstructure was analyzed by Scanning Electron Microscopy (SEM) coupled with Energy Dispersive X-ray Spectroscopy (EDS). As shown in Figure III – 1 (a and b), the produced fracture surfaces were divided into 9 different sections within the anode

thickness, position 1 and 9 corresponding to the outer portion and the anode/electrolyte interface, correspondingly. For each section, Cu and Ce content was evaluated and comparison was made between cells before and after the electrochemical characterization.

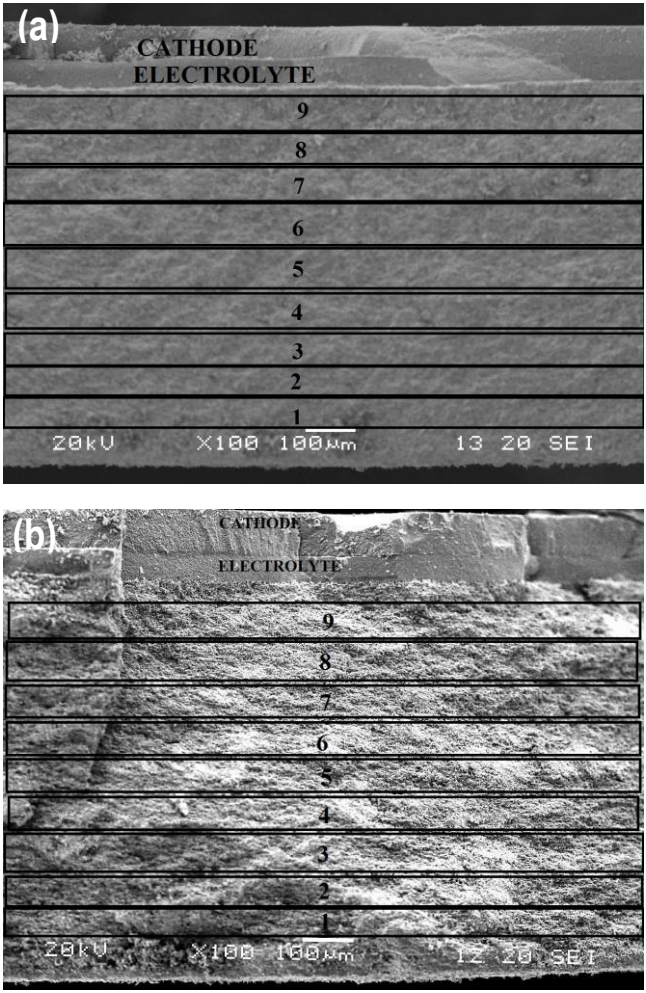

Figure III – 1 Fracture surface of (a) 35 vol%15 and (b) 45 vol% CuO-containing anode-supported SOFC

3.2.8 Analysis of catalytic activity of GDC

The reducibility of CuO and GDC was studied by reduction at controlled temperature (H_2-TPR) by using a Thermo TPR/R/O 1100. The sample (≈30 mg) was introduced in a quartz reactor placed in a tubular furnace. The furnace temperature was increased up to 850 °C (10°C/min), while a flux made of 5 vol% H_2 in Ar (30 mL/min) was employed. The reaction between the hydrogen and the sample were detected by a thermal conductivity detector (TCD).

The quartz reactor (8mm DI) was placed in a tubular furnace controlled by a PID. The gas chromatograph used for gas analysis (Agilent 7890) was equipped with a column Molecular Sieve X13 (for H_2, Ar, CO and CH_4 separation) e by a Hayesep Q column (per CO_2). The gas was analysed by a TCD revealer.

Two different reactions were studied:

$$CH_4 + CO_2 = 2H_2 + 2CO (3{,}1)$$

$$2CH_4 + O_2 = 4H_2 + 2CO \ (3.2)$$

The catalyst (200 mg) was activated by reducing in H_2 (700°C, ca. 30 min). For the the reaction 3.1 (Dry reforming of Methane, DRM) was employed a gas mixture of 100 mL/min with a volume ratio CH_4:CO_2:N_2:He=10:10:20:60, while for the reaction 3.2 (Partial oxidation of Methane, POM) a gas mixture of 100mL/min with a volume ratio of CH_4:CO_2:N_2:He =10:1:20:69 was used.

The reactant conversion was calculated through the gas composition by the eq:

$$X_i(\%) = 100 \left(1 - \frac{C_i \, C^0{}_{N_2}}{C^0{}_i C_{N_2}}\right) (3.3)$$

Where X_i represents the reactant conversion (i=CH_4, CO_2 e O_2), $C^0{}_i$ and C_i are the input and output cocentrations, respectively.

Chapter IV

Results and discussion

Part of this chapter has been published in:

ECS Transaction,

"Effect of Bismuth Oxide as Sintering Aid for Gadolinia-doped Ceria at 1050°C",
Volume 68, issue 1 (2015), 413-420

Ceramic Engineering and Science Proceeding,

"Production and co-sintering at 950°C of planar half-cells with CuO-GDC cermet supporting anode and Li_2O-doped GDC electrolyte",
Volume 37, Issue 3 (2016), 31-38, The American Ceramic Society

Journal of Power Sources

"Production of planar copper-based anode supported intermediate temperature solid oxide fuel cells cosintered at 950°C"
vol. 328, pp. 235-240, 2016.

Journal of the Ceramic Society of Japan

"Performance and evolution of planar copper-based anode-supported solid oxide fuel cells"
Volume 125 [4] 313-316 2017

International Journal of Hydrogen Energy

"Effect of anode thickness and Cu content on consolidation and performance of planar copper-based anode-supported SOFC"
To be published doi: 10.1016/j.ijhydene.2017.03.221

Fuel Cells

"Influence of copper-based anode composition on intermediate temperature solid oxide fuel cells performance"
To be published

4.1 Production of Gadolinia-doped Ceria dense electrolyte

4.1.1 Analysis of viscosity

As described in chapter 3, the dispersant amount was optimized by using the viscosimetric tests[47]. It was examined by measuring the viscosity in an Active Part (AP) range between 0 and 1.25 mg m^{-2}. The viscosity for AP=0 has not been evaluated, since the slurry does not presented as a viscous fluid but as powder agglomerated and thickened, similar to a dough. The starting Solid Load (SL) was chosen based on the lab experience, this suggesting a SL between 16 and 20 vol%, in order to provide a suspension more viscous than water but not too dense. General results are shown in Figure IV – 1.

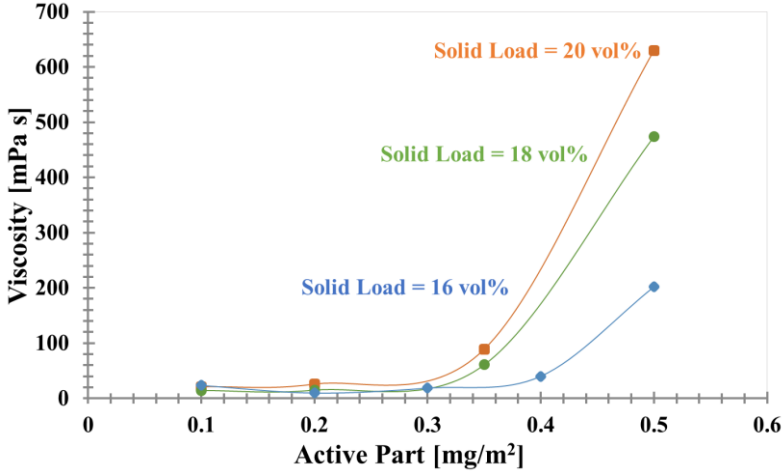

Figure IV – 1. Slurry viscosity as a function of dispersant content (AP) and solid load (SL)

As one can observe in Figure IV – 1, the minimum viscosity, for GDC powders with particle size and SSA equal to those used in the laboratory, is obtained in an AP range particularly low, equal to 0.1 – 0.3 mg m^{-2}, for each SL value. The absolute minimum was obtained for PA ≈ 0.2. However, for problems related to the suspension pH, the maximum PA allowing to remain in the minimum viscosity range (PA=0.3) was chosen.

4.1.2 Additives optimization

The amount of additives in the suspension was properly fixed, due to the onset of two main problems:

1. cracking of the green
2. instability of the suspension during mixing

To improve the first aspect many tests at increasing the active part of the additives were performed. Through various analyses, it was verified that the optimum ratio between the active parts of binder and plasticizer should be about 1:1. If the ratio of the two additives changes, the tape presents a high risk of cracking for the high stiffness, when the ratio is in favor of the binder, or poor mechanical strength, when it was in favor of the plasticizer. Once optimized the ratio between the additives AP, the minimum quantity to be introduced within the suspension to obtain a green with the desired properties was defined. A minimum value of additives to be included in the slurry was identified, in order to eliminate the cracks in the drying step, for AP of both binder and plasticizer variables in the range between 5 - 6.

4.1.3 Tape casting process

The difficulty to draft the thin-film suspension by tape casting depends on the rheological properties of the slurry. If the suspension is not perfectly homogeneous or contains large clumps, this will not result in a good tape. Furthermore, the drying process of the aqueous material, immediately subsequent to the casting, is somewhat problematic. In fact, the water has a high evaporation rate, and if the process is not governed, it can affect not only on the quality of the green, but especially on its integrity (Figure IV - 2). Therefore, the thickness of the deposited material plays a very important role; if it is too high, the drying will take place with a high velocity gradient between the surface exposed to air of the film with respect to that on the surface in contact with the support material; this will lead to a deformation of the non-isotropic material. The effect of this lack of homogeneity in shrinkage upon drying can be partially eliminated by inserting a large amount of additives such as binder and plasticizer. However, to obtain a green and accordingly a sintered material with good properties, the amount of additives should be limited to the minimum necessary. For this reason, if the drying takes place in a controlled manner, it will be possible to obtain a smooth layer. An approach to achieve the water evaporation in an optimal way is therefore to reduce the film thickness. Initially it was used a height, of the blades of the doctor blade, measured relative to the support material, of 300 μm, which corresponds to a thickness of the ceramic film (green) of about 150 μm after drying. For the above mentioned reasons this thickness was reduced to 200 microns. Such choice allowed eliminating many macroscopic defects of the dried material, as shown in Figure IV - 3. Samples sintered at 1550°C for 3 h (diameter = 30 mm) were analysed, after being

manually but carefully fractured along the thickness. The additives amount was optimized in the GDC slurry production. The optimization of the dispersant and of the others additives allows to achieve a gas tight microstructure, as shown in Figure IV - 4 and Figure IV - 5.

Figure IV – 2. Cracked green material because of an incorrect drying process

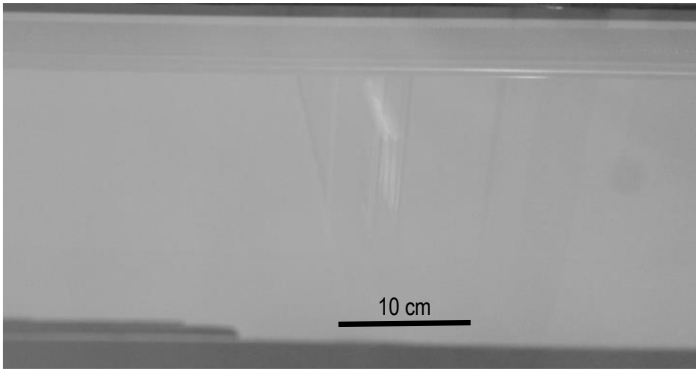

Figure IV – 3. Defect free green surface

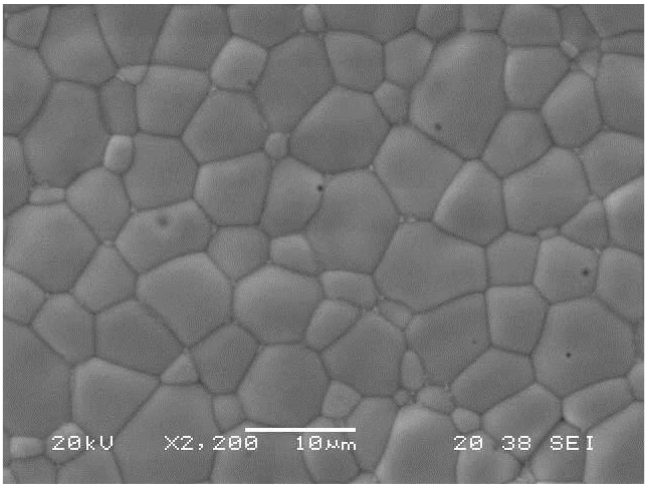

Figure IV – 4. Cross surface of a GDC sample sintered for 3h at 1550 °C

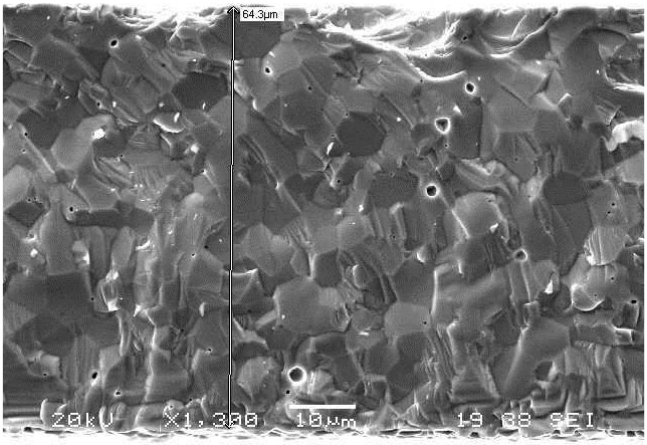

Figure IV – 5. Fracture surface (produced by manual fracture) of a GDC sample sintered for 3h at 1550 °C

4.2 *Effect of Bismuth Oxide as Sintering Aid for Gadolinia-doped Ceria at 1050°C*

The effect of the bismuth oxide as sintering aid on shrinkage (ε) and shrinkage rate (dε/dt) of GDC10 is shown in Figure IV - 6 and Figure IV - 7.

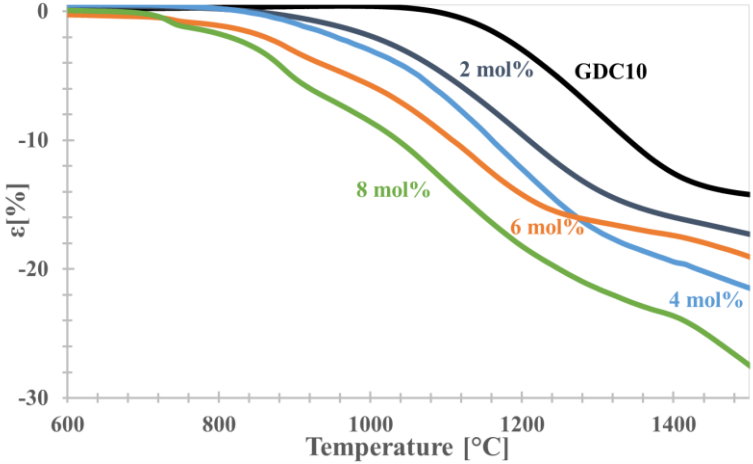

Figure IV - 6. Effect of Bi_2O_3 on the GDC10 sintering behaviour, measured at 10°C/min in air.

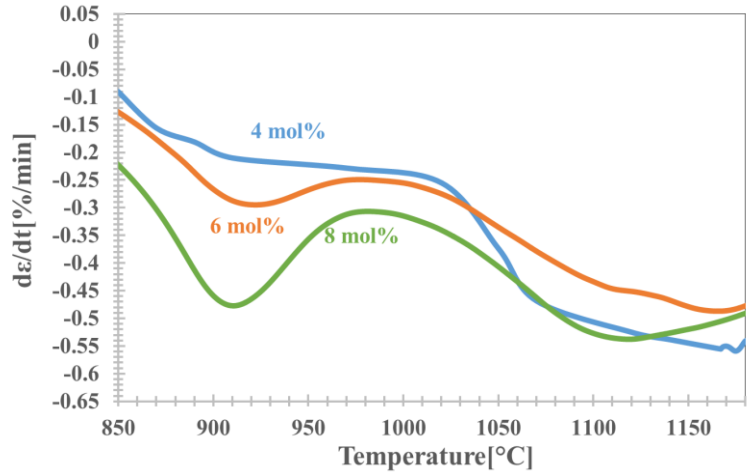

Figure IV - 7. Shrinkage rate curves for three different Bi_2O_3 loads.

There is an evident effect on the sintering onset temperature which decreases from about 1100°C for pure GDC10 to less that 800°C when 6-8 mol% Bi_2O_3 is added. The

shrinkage rate changes substantially in the presence of Bi_2O_3, especially for loads in excess to 6 mol%: for lower content, the minimum shrinkage rate (i.e maximum sintering rate) is recorded at about 1100-1200°C; conversely, for dopant concentration of 6 and 8 mol% two additional minima for (dε/dt) are shown at ≈730°C and ≈880°C. This points out that additional mechanisms for sintering are activated, probably correlated with phase changes in the GDC-Bi_2O_3 system occurring at such temperatures when Bi_2O_3 concentration is sufficiently high.
The effect of sintering holding time at 1050°C on apparent porosity is shown in Figure IV - 8.

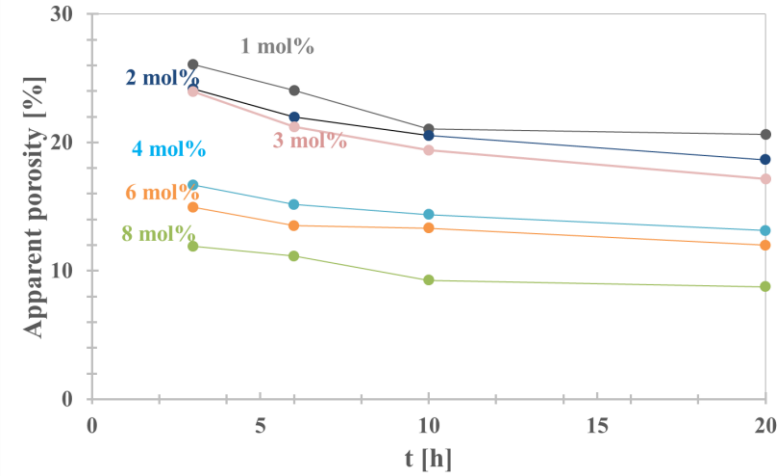

Figure IV - 8. Effect of different holding time and Bi_2O_3 load on GDC10 apparent porosity for sintering at 1050°C.

As expected, the apparent ("open") porosity decreases monotonically as the holding time is increased. This accounts for denser samples and more limited closed porosity. The sum of the apparent porosity and relative density is always in excess to 95% after 20 h sintering, thus leading to closed porosity values lower than 5%. On this basis, the open porosity represents the key parameter to detect how the Bi_2O_3 content affects the GDC10 sinterability. From Figure IV - 8, one can observe that samples containing 6 mol% Bi_2O_3 show the lowest apparent porosity for any holding time at 1050°C.
The apparent porosity trend are consistent with the relative density data, shown in Figure IV – 9.

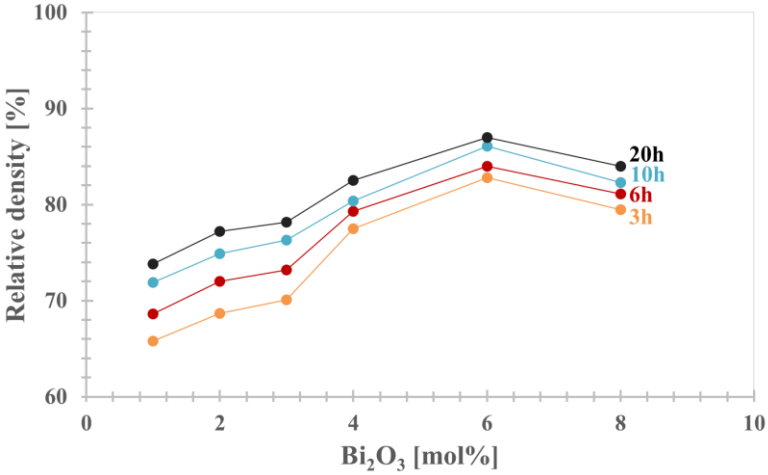

Figure IV - 9. Relative density as a function of Bi_2O_3 content after sintering at 1050°C for different holding time.

One can observe that the relative density increases with Bi_2O_3 load up to 6 mol% and then decreases. The same is true for the radial shrinkage (Figure IV-10), which is maximum at 6 mol% Bi_2O_3 content.

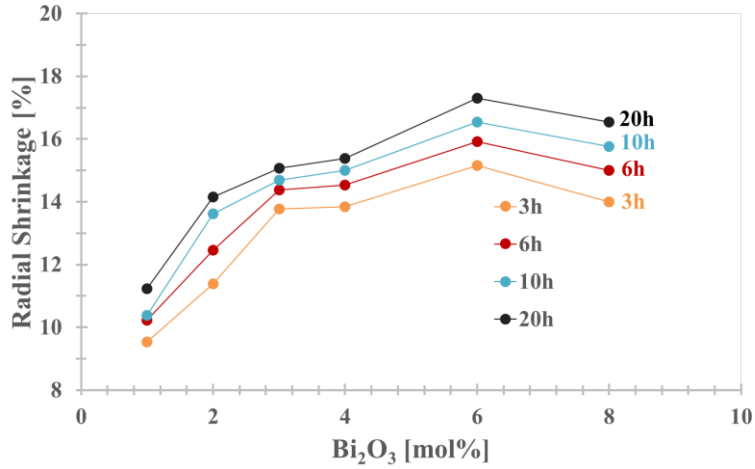

Figure IV – 10. Radial shrinkage as a function of Bi_2O_3 content after sintering at 1050°C for different holding time.

These results are partially unexpected if the dilatometric results (Figures IV-6 and IV-7), pointing out a monotonically increasing shrinkage and shrinkage rate with dopant content, are considered. One should however consider that dilatometric analysis is

performed under constant heating rate condition and, therefore, the holding at 1050°C appears to have a more important effect on final density and porosity.
The observation of the fracture surfaces allows to point out the improved densification caused by the addition of 6 mol% Bi_2O_3. It has to be stated that, although 8 mol% showed a densification equal or not significantly higher than 6 mol%, it is preferable to keep the doping at a lower value, in order to affect as less as possible the ionic conductivity property of the compound, the aim being the production of a GDC-based electrolyte. From the observations of the fracture surfaces, the improved sintering caused by both different doping and different holding time is clear (Fig. 11). Figure IV-11 (a) shows the effect of 2 mol% Bi_2O_3 doping after 3 h at 1050°C. It is easy to observe how the structure corresponds to the starting sintering stage and almost no flat contacts among particles or grain boundaries are present. The situation improves after 10 h (Figure IV - 11(b)) for the same doping concentration while sintering is in an advanced stage in Figure IV - 11(c), where the structure of 6 mol% Bi_2O_3-containing sample after 10 h is shown; here, the porosity is isolated and sintering is moving towards the final stage.

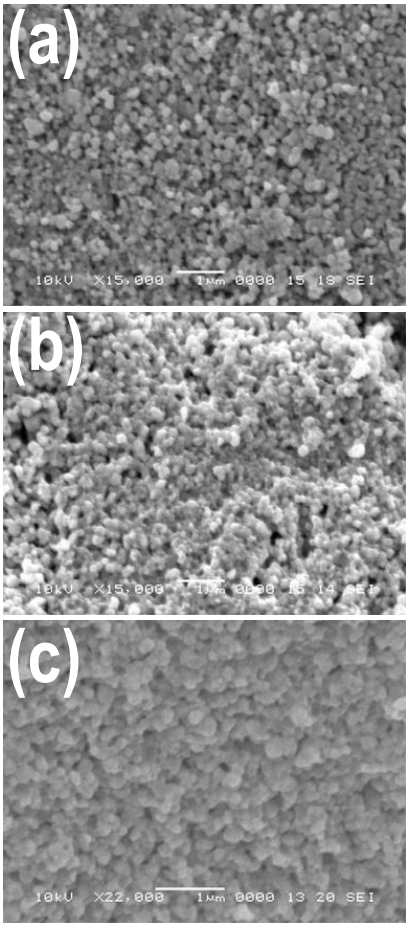

Figure IV - 11. Fracture surface of (a) 2 mol% Bi_2O_3-containing sample sintered for 3 h, (b) 2 mol% Bi_2O_3-containing sample sintered for 10 h and (c) 6 mol% Bi_2O_3-containing sample sintered for 10 h (sintering temperature = 1050°C).

4.3 Effect of Lithium Oxide as Sintering Aid for Gadolinia-doped Ceria

The effect of Li_2O on GDC10 pellets sintering behavior is shown in Figure IV-12

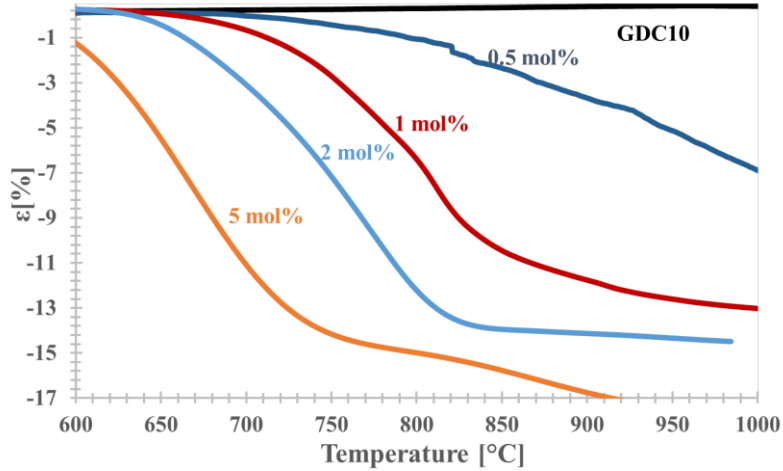

Figure IV - 12. Effect of Li_2O on GDC10 sintering behavior (deformation, ε, as a function of temperature).

An evident decrease of the onset temperature can be pointed out, this decreasing from about 1100°C for pure GDC10 to ≈ 600°C when 5 mol% Li_2O is added. Samples containing 2 mol% and 5 mol% Li_2O-doping show a full densification at ≈ 950°C and at ≈ 850°C, respectively. Therefore, with regard to the fundamental requirement related to the aim of the present work, i.e. reduce the GDC sintering temperature below the CuO melting point, Li_2O-content equal to 2 mol% could be sufficient to achieve sintering at 900°C. The promising results allowed to produce Li-GDC based electrolyte through water-based tape casting. Nevertheless, the doping effect needs to be amplified as much as possible; as a matter of fact, the dilatometric curves in Fig. IV-12 are referred to cylindrical pellets contain only powder while tape casting suspension, has a much lower solid content, not reaching 20 vol%. Thus, the complete densification is partially inhibited (probably due to the distance between powder particles). Consequently, in order to obtain similar densification, larger amount of sintering aid is required. Moreover, in previous works[20, 48], 2 mol% Li_2O doping resulted sufficient to achieve almost fully densified GDC-based electrolyte in tubular copper-based anode supported IT-SOFC only at 1020°C.

The powder chosen for producing the electrolyte is the 5 mol% Li_2O-doped GDC. The limited SL lower than 20% makes the reaching of fully dense monolithic electrolyte at the desired temperatures (950°C) not possible, as shown in Figure IV - 13.

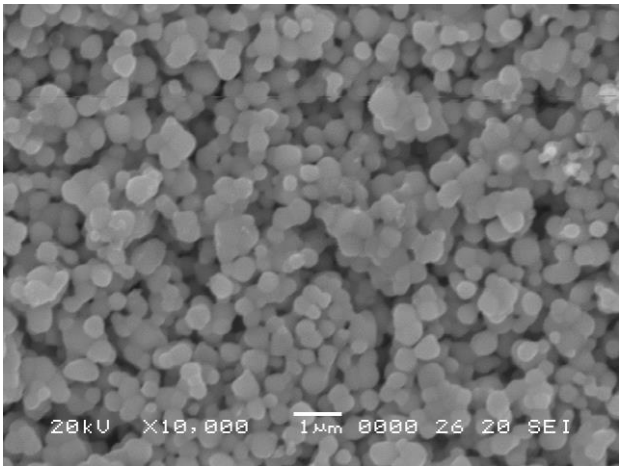

Figure IV - 13. Cross section (produced by manual fracture) of 5 mol% Li_2O -doped stand-alone tape cast sample sintered at 950°C.

Therefore, samples obtained by tape casting need an additional sintering aid to achieve densification at the desired temperature. Such aim was identified in the mechanical effect of the supporting anode. In fact, when a Cu-containing supporting anode is coupled with the electrolytic layer, gas tight microstructure can be achieved, this being accounted for by the different shrinkage rate ($d\varepsilon/dt$) between the two layers that develops compressive stresses upon sintering in the thinner (electrolyte) one. Such stresses can be expressed as[49]:

$$d\sigma/dt = E\left(\frac{d\varepsilon}{dt_{el}} - \frac{d\varepsilon}{dt_{an}}\right) \quad (4.1)$$

where E is the electrolyte Young's Modulus, $d\varepsilon/dt_{el}$ eland $d\varepsilon/dt_{an}$ the shrinkage rate of the electrolyte and of the anode, respectively. When the anode is the faster shrinking layer (i.e., when $\frac{d\varepsilon}{dt_{el}} - \frac{d\varepsilon}{dt_{an}} > 0$), the stress state described by Eq. (4.1) is compressive and activates the densification. The behaviour of different CuO-GDC cermet anode-supporting half-cells both in the heating and in the cooling stage of sintering was compared. Such half-cells were produced by coupling the 2 mol% Li_2O-doped GDC10 electrolyte with the anodes, whose composition is summarized in Table IV-1.

Figure IV - 14 shows the shrinkage rate of the electrolyte and of "A" and "B" anodes.

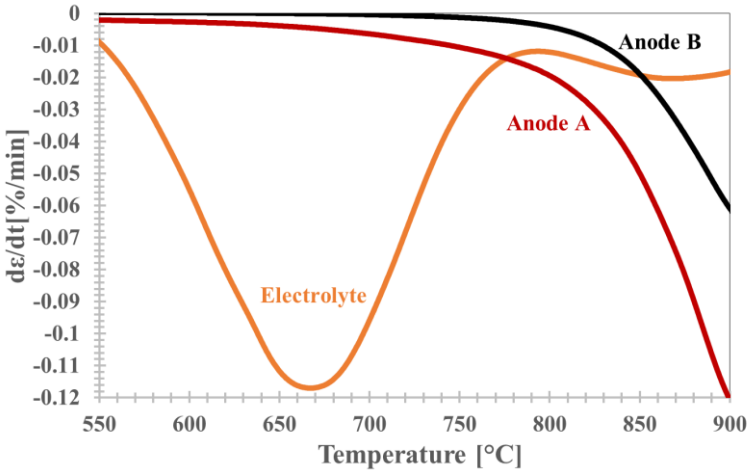

Figure IV - 14. Anode and electrolyte shrinkage rate upon sintering.

Such cermets are characterized by the same relative amount of metallic and ceramic oxides, but in Anode "A" the ceramic part is 2 mol% Li_2O-doped GDC10, while in Anode "B" undoped GDC10 is used. As one can observe, in the former case it is possible to achieve an earlier sintering and, consequently, a larger shrinkage rate (i.e., lower $\frac{d\varepsilon}{dt}_{an}$) at the same temperature. Therefore, according to Eq. 4.1, if anode "A" is considered, the electrolyte starts being in a compressive tensile state at a temperature ≈20°C below (at ≈850°C instead of ≈870°C), this allowing to obtain the desired sintering before. This suggested to use Li-doped GDC10 for the ceramic part of the anode.

The Thermal Expansion Coefficient (TEC) is the parameter that has to be considered to fix the amount of metallic oxide in the anode. A TEC mismatch between two coupled layers gives rise to thermal strain (ε_{res}) upon cooling, which result in residual stresses. At a first approximation, the strain is equal to[50]:

$$\varepsilon_{res} = \int_{T_{room}}^{T_{stress\ free}} (\alpha_{an} - \alpha_{el})\, dT \qquad (4.2)$$

where T_{room} is the room temperature, $T_{stress\ free}$ the stress free temperature (always lower than sintering temperature)[51-53], α_{an} and α_{el} are the anode and electrolyte TEC, respectively. Therefore, according to Eq. 4.2, a larger TEC mismatch is responsible for larger strains and residual stresses. If the stresses are larger than the material resistance, surface cracks are developed, thus compromising the cell integrity, as shown in Fig. IV-15, where the electrolyte was coupled with anode "C", containing 40 vol% CuO. Thus, by reducing the CuO content from 40 vol% to 30 vol% (Anode "A"),

the TEC mismatch is strongly minimized and the strain is limited and a defect free electrolyte can be obtained (Figure IV-16). Figures IV - 17 shows how an almost fully dense electrolytic microstructure (with closed porosity) was obtained by coupling and sintering the anode "A" with the electrolyte; Figure IV – 18 shows a cross section of the entire half-cell.

As a general conclusion, it is possible to state that, to achieve the GDC densification at a temperature compatible with che CuO melting point, a 5 mol% Li_2O-doping is needed in the electrolyte tape casting recipe and the additional aid of the supporting anode is also required. Moreover, a certain amount of Li-doping is necessary in the Cu/GDC anodic cermet to further enhance the electrolyte densification.

Table IV – 1 Composition of the electrolyte and of the tested anodes.

	Relative amount [vol%]		
	5 mol% Li_2O-doped GDC10	Undoped GDC10	CuO
Electrolyte	100	0	0
Anode A	70	0	30
Anode B	0	70	30
Anode C	60	0	40

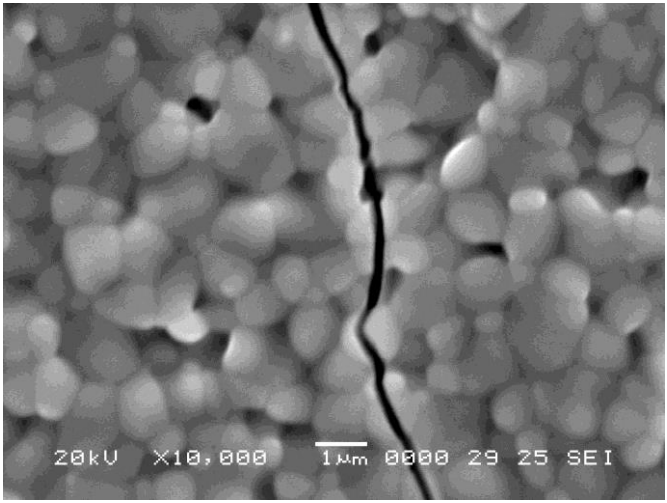

Figure IV - 15. Electrolyte surface after cosintering with anode C for 3 h at 950 °C.

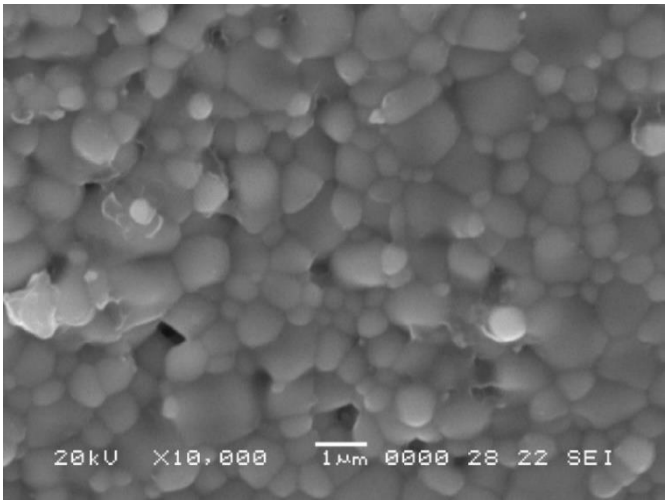

Figure IV - 16. Electrolyte surface after cosintering with anode A for 3 h at 950°C.

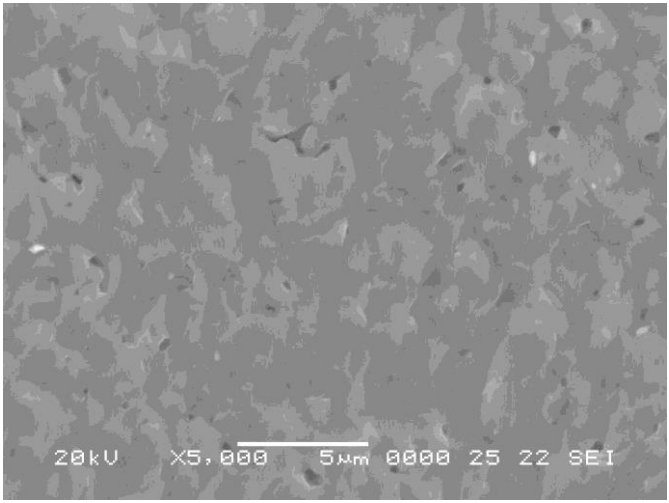

Figure IV - 17. Cross section (produced by manual fracture) of the electrolyte after cosintering with anode A for 3 h at 950°C.

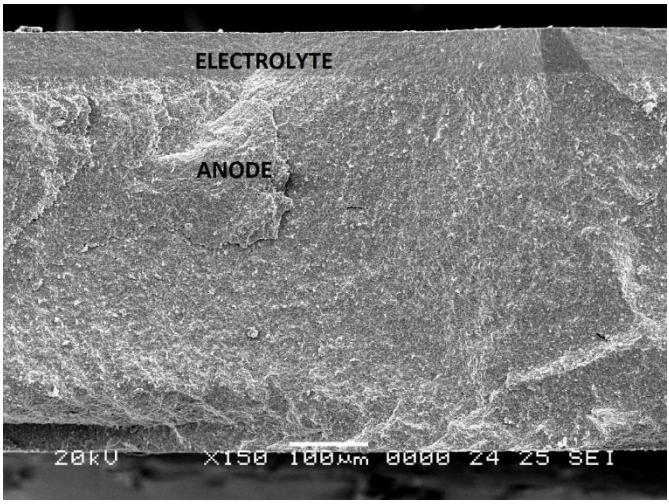

Figure IV - 18. Cross section (produced by manual fracture) of the half-cell cosintered for 3 h at 950°C.

4.4 CuO and GDC reduction by TPR

Fig IV – 19 reports the TPR profiles of 45 and 50 vol% CuO containing cermet.

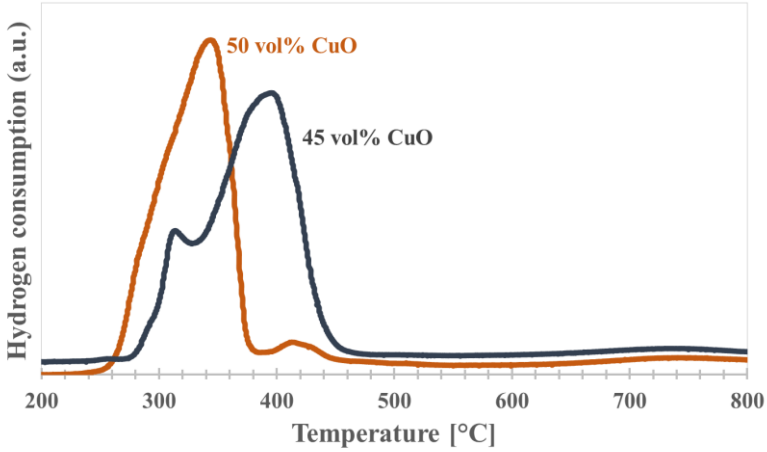

Figure IV – 19. H_2-TPR profiles of 50 and 45 vol% CuO containing cermet).

Both samples show two reduction peaks within the range 250-450°C, this being likely due to the reduction: $CuO+H_2= Cu^0 + H_2O$[54, 55].

In detail, the 50 vol% CuO containing sample shows the highest peak at T= 340 °C and a less intense peak at T= 413 °C, while, for 45 vol% CuO, the highest and the lowest peaks are at T= 395 °C and T= 313 °C, respectively. At high temperature (≈740°C), both samples reveal another limited peak, more evidenced in Figure IV – 20, this being accounted for the reduction of Ce^{4+} to Ce^{3+} in GDC.

As known, CeO_2 and solid solutions reduction rate strongly depends on the oxide morphology[50, 51].

Sub–micron and nano-structured materials, with high SSA, reveal reduction peaks at relatively low temperature, due to the $Ce^{4+} \rightarrow Ce^{3+}$ reduction of nanoparticle surface, and reduction peaks at high temperature, due to the bulk reduction. Even the amount of H_2 reacted, proportional to the moles of Ce^{4+} reduced, depends on the morphology of the material. In general, sintered $Ce_{(1-x)}\ M_{(x)}O_y$ show only high temperature peak (>600 °C), due to the bulk reduction. Based on such results, it is possible that the use of GDC based electrolyte at a temperature above 700°C becomes detrimental for the performance, in particular for a possible OCV reduction. The tested samples had a sintering process at 950 °C, this leading to a limited surface area and, therefore, to a low intensity peak.

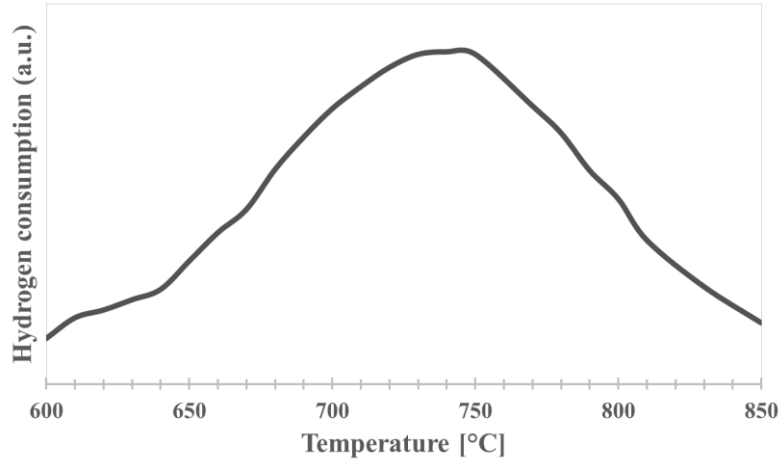

Figure IV - 20. H_2-TPR profiles of 45 vol% CuO containing cermet. Detail of the Ce reduction

4.5 Electrochemical screening

4.5.1 Cell tests in H_2

4.5.1.1 Effect of CuO concentration

Fig. IV - 21 shows the performance of the 25 vol% CuO-containing IT-SOFCs.

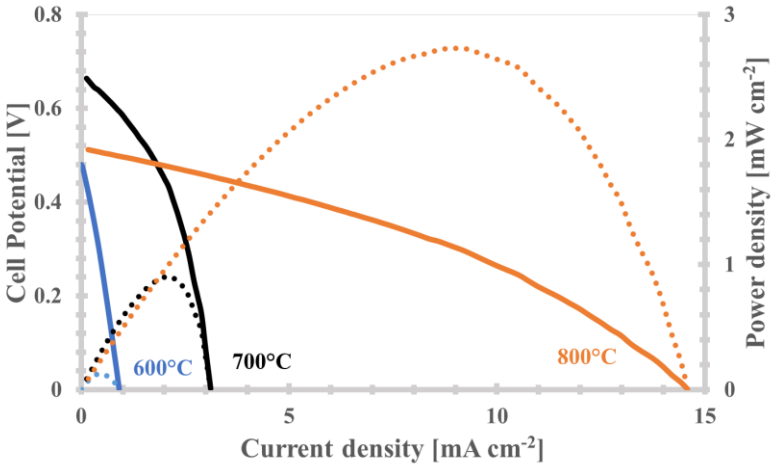

Figure IV - 21. Cell Potential and Power Density vs. Current Density of the 25 vol% CuO containing SOFC, at different temperatures.

In this cell, the GDC used for the electrolyte is doped by 5 mol% Li_2O. The results here shown are referred to the first cell produces. Consequently, they are really poor. Despite this, an interesting consideration can be made on the Open Circuit Voltage. As one can observe, the OCV varies in a certain range (between 0.5 V to 0.7 V) and this, in addition to the experimental error, can be probably accounted for by some electronic conductivity induced in GDC by the reduction of CeO_2 to Ce_2O_3 predicted by Fig. IV – 20 and/or deformations induced by such reduction reactions or caused by the thermal mismatch which can generate micro-flaws and leakages in the electrolyte.

The electrolyte cross section is shown in Figure IV – 22. The low densification is the major responsible of the huge impedance, as revealed by Figure IV – 23, where the impedance spectrum at 600°C is reported.

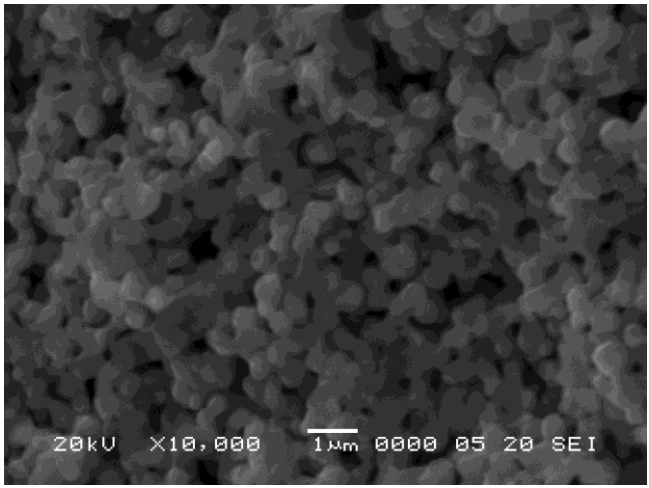

Figure IV - 22. Electrolyte cross section (produced by manual fracture) of the 25 vol% CuO containing planar SOFC sintered at 950°C

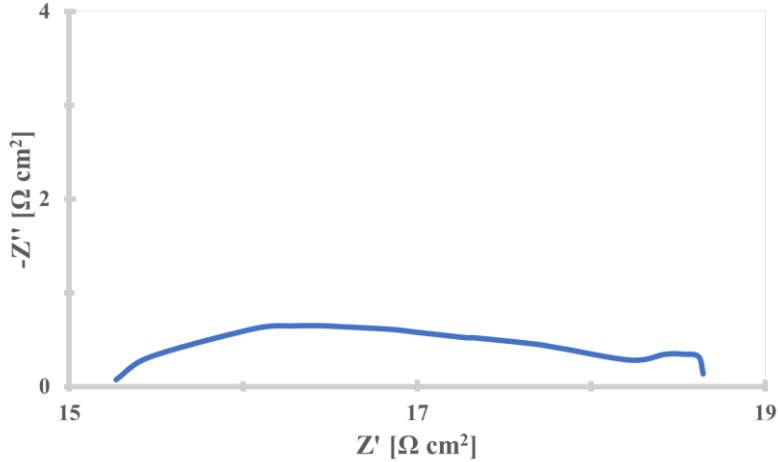

Figure IV - 23. Impedance spectrum of 25 vol% CuO-containing cell at 600°C

An increasing of CuO content within the anodic cermet allows to strongly improve the SOFC performance. Figure IV - 24 shows the electrochemical performance of the 35 vol% CuO containing cell at different temperatures between 550°C and 650°C.

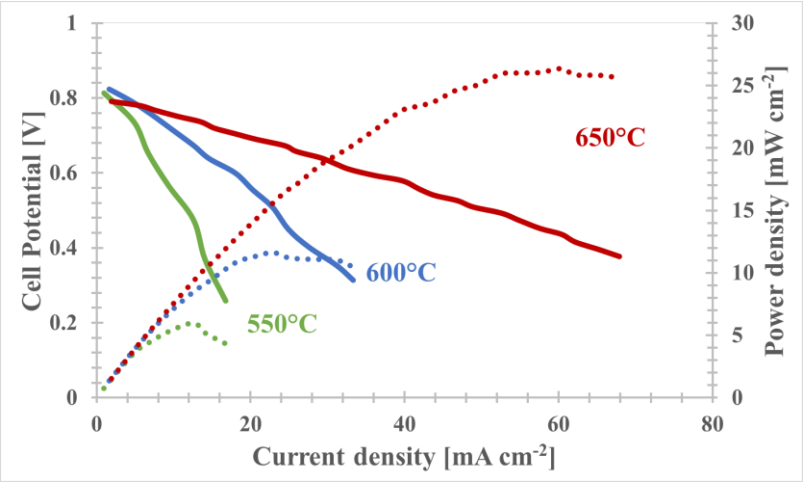

Figure IV - 24. Cell Potential and Power Density vs. Current Density of the 35 vol% CuO containing SOFC, at different temperatures.

For the operating condition, the theoretical Nernst potential is about 1.1 V. As one can observe, the OCV is nearly constant at ≈ 0.8 V. According with the literature[13], the addition of lithium should not account for any electronic conductivity, this suggesting that the difference between experimental and theoretical OCV could be due related to other factors, such as residual leakages in the electrolyte and the dense anode that does not allow the complete H_2 flow towards the active sites. At 550°C the cell achieves power density of ≈ 6 mW/cm^2 at current density of 13 mA/cm^2. Power density increases with testing temperature reaching 26 mW/cm^2 at 70 mA/cm^2. This behaviour seems to be qualitatively consistent with experimental results obtained on similar SOFC previously reported[58,59]. Despite the lithium doping concentration was increased up to 5 mol% in the electrolyte, this further favourating the GDC sintering, the 35 vol% CuO-containing cell still shows a relatively limited maximum power density, this being very likely associated to the relatively large electrolyte thickness and the high electrodes densification that are responsible for the ohmic resistance shown in figure IV-25. Figure IV – 26 shows the cross section of the whole 35 vol% CuO cell.

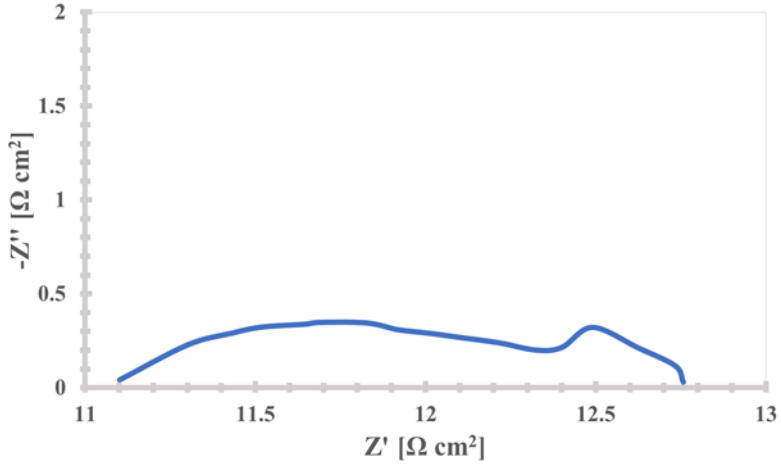

Figure IV - 25. Cell impedance measured at 600°C of the 35 vol% CuO containing SOFC.

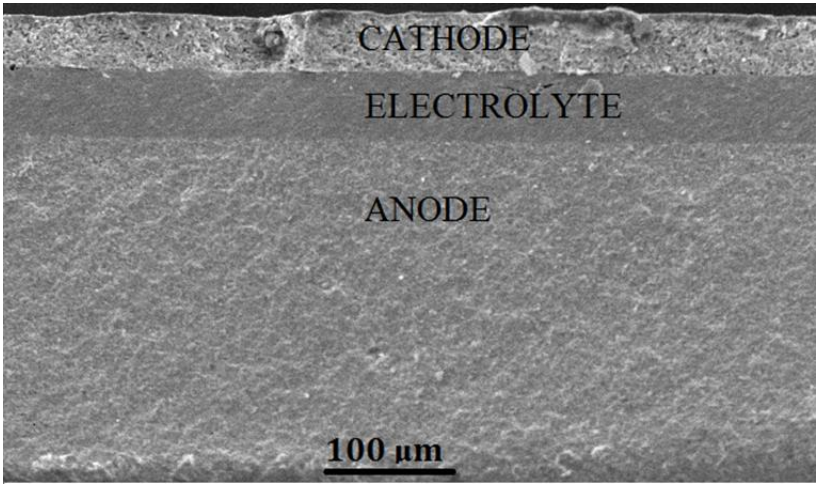

Figure IV - 26. Cross section (produced by manual fracture) of the 35 vol% CuO - containing SOFC sintered at 950°C

The overall performances can strongly improve if the copper load within the anodic cermet is further increased.

Figure Fig. IV – 27 shows the polarization and power density curves for 35, 45 and 50 vol% CuO-containing cell at 600°C.

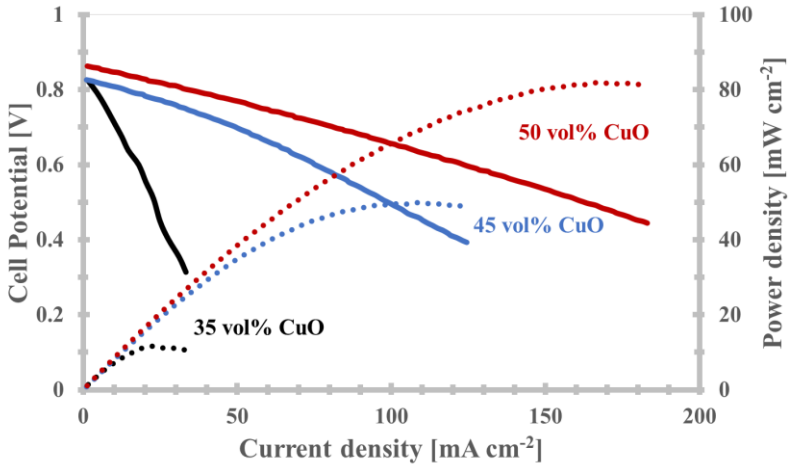

Figure IV – 27 Polarization and power density curves for 35, 45 and 50 vol% CuO-containing cell at 600°C.

One can observe a significant increase of the overall cell performance with Cu load: maximum power density increases from ≈ 12 mW cm^{-2} up to ≈ 80 mW cm^{-2} for CuO content varying from 35 to 50 vol%. Similar behaviour was observed also at 650°C and 700°C for cells containing at least 35 vol% CuO. Maximum power density values achieved in different operating conditions are summarized in Table IV – 2.

Table IV - 2 Maximum power density for 35, 45 and 50 vol% CuO-containing cells at different temperature.

CuO content [vol%]	Temperature [°C]	Power density [mW cm^{-2}]
35	600	12
	650	26
	700	40
45	600	50
	650	100
	700	140
50	600	80
	650	140
	700	200

Interestingly, values as high as 140 and 200 mW cm^{-2} are recorded at 700°C for cells containing 45 and 50 vol% CuO, respectively. Fig. IV - 27 points out a clear OCV improvement (> 0.8 V) that is accounted for a better electrolyte densification, as shown

in Fig. IV - 28. There is a clear influence of Cu content in the anode on the electrolyte densification: for 25 vol% CuO containing-cell, the electrolyte remains a bit porous and some limited open channels could probably account for the prevopusly hypothesized leakage; conversely, the electrolyte in cells containing at least 35 vol% CuO are substantially completely densified. The observed behaviour can be related to the development of different stress regimes in the electrolyte for variable CuO content in the anode upon sintering: it is very likely that the densification of the anode is accelerated for larger CuO content and this induces a certain compression in the electrolyte which, therefore, sinters better.

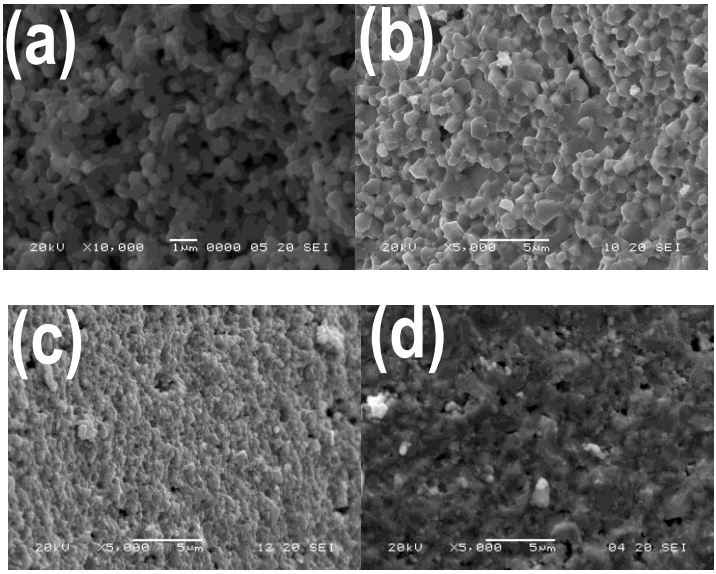

Figure IV – 28 Electrolyte fracture surface (produced by manual fracture) of 25 (a), 35 (b), 45 (c) and 50 vol% (d) CuO-containing cells.

With reference to the equivalent circuit in Figure IV – 29, electrochemical impedance spectroscopy results for the above mentioned cells are reported in Figure IV – 30.

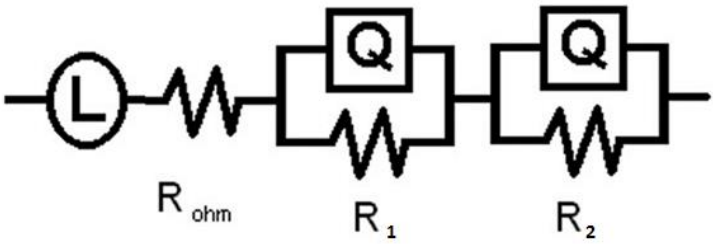

Figure IV – 29 Equivalent circuit employed for the impedance spectrum evaluation (L = inductance, due to the testing system; R_Ω = ohmic resistance, R_1= charge transfer resistance on the interface region, R_2 = passive layer impedance, Q = constant phase element)

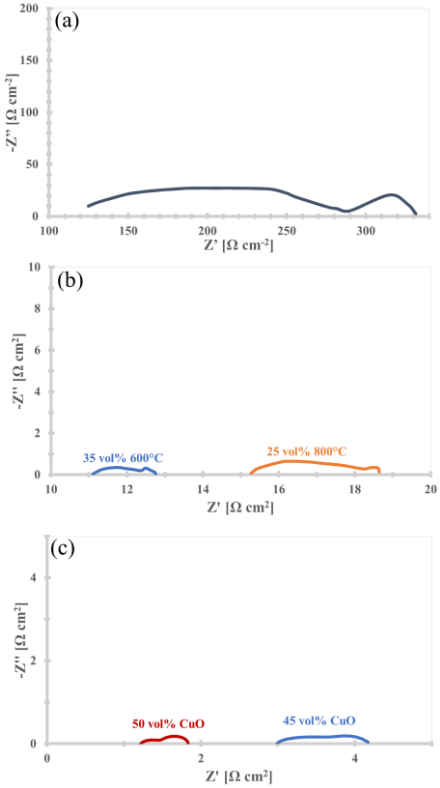

Figure IV – 30 EIS spectra for (a) 35 vol% CuO-containing cell at 600°C, (b) 35 vol% CuO-containing cell at 800°C and 25 vol% CuO-containing cell at 600°C, (c) 45 and 50 vol% CuO-containing cell at 600°C.

R_1 is typically represented by the high frequency arc[66], while R_2 corresponds to the low-frequency arc. The intercept at high frequency is associated with R_Ω[62]. The performance of 25 vol% CuO-containing cell improves by increasing the operating temperature (Figure IV – 30(a-b)), R_Ω decreasing from ≈ 120 Ω cm^2 at 600°C to ≈ 15 Ω cm^2 at 800°C. This result is consistent with the R_Ω dependence on temperature. Nevertheless, EIS spectra point out a better polarization for 35 vol% CuO-containing cell with respect to 25 vol% CuO-containing one. Both the ohmic and the electrodes resistances further reduce if 45 and 50 vol% CuO containing cell are considered (Figure IV – 30(c)).

Since all cells were assembled with the same cathode and electrolyte, R_1 and R_2 differences shall be mainly accounted for by the anodic reactions. For 25 vol% CuO – containing anode, R_1 is equal to 176 Ω cm^2, this confirming the limited performances shown by the I-V curve. R_1 strongly decreases by increasing the CuO content up to 50 vol%, this being equal to about 2.2, 0.3 and 0.4 Ω cm^2 for 35, 45 and 50 vol% CuO-containing cells, respectively: the beneficial effect of CuO on anode conductivity is therefore clear. Since R_1 shows a plateau, 45-50 vol% CuO corresponds to suitable anodic composition for SOFC operating at 600°C. Some cells were also produced by using 55 vol% CuO in the anodic layer. Unfortunately, such cells are characterized by the presence of cracks within the electrolyte, which cause macroscopic leakages, accounted for by thermal expansion coefficient mismatch between anode and electrolyte upon cooling after sintering[42]. This result suggests that 50 vol% CuO load shall not be exceeded in the realization of the anode in the considered cell configuration.

The effect of temperature on EIS behaviour was therefore investigated in detail for 45 and 50 vol% CuO-containing cells. Here, the effect of the constant phase element (CPE) was also considered for a more comprehensive analysis of the collected spectra. CPE impedance is typically expressed as:

$$Q = \frac{1}{Y_0(j\,\omega)^n} \qquad (4.3)$$

where Y_0 is a frequency-independent constant, ω the angular frequency (ω = 2 π f, f= frequency), $j=(-1)^{0.5}$ and n an exponent which identifies the element: for n equal to 1, 0.5, 0, and −1, Q represents an ideal capacitance, a Warburg impedance, an ideal resistance and an inductance, respectively[8]. The results of the EIS spectra fitting are collected in Tables IV – 3 and IV - 4. For both cells, R_Ω decreases by more than 60% if the operating temperature varies from 600°C to 700°C, this confirming the trend already observed for 25 vol% CuO-containing cell. Analogously, R_1 decreases by ≈ 80%. As expected, R_2 is much more sensitive to temperature variations[80]. In fact, its reduction is more than 95% in both cells. Moreover, it is possible to observe how the constant phase element has behaviour closer to an ideal capacitance for increasing temperature. The effect of temperature can be mainly appreciated by considering the Bode plots for the two selected cells (45 and 50 vol% CuO) reported in Figure IV – 31.

The peak in the low frequency range (below 100 Hz) can be ascribed to the mass transfer phenomena[81]. Better performances are obtained by employing larger CuO load, even at much lower temperature, this indicating a strong chemical dependence of the resistance parameters on anodic cermet composition.
As an overall result, 50 vol% CuO content in the GDC anode can be identified as an optimal compromise between electronic conductivity, catalytic activity and thermal expansion mismatch among the different layers. The overall cell resistance parameters are absolutely comparable with those reported in previous works for conventional Ni-based anodes[82, 83], despite the absence of the catalytic activity provided by Ni.

Table IV - 3 EIS fitting results for 45 vol% CuO-containing cell at different temperature

T [°C]	R_Ω [Ω cm^2]	R_1 [Ω cm^2]	n1	R_2 [Ω cm^2]	n2
600	2.86	0.31	0.8	1.04	0.6
650	1.11	0.17	0.9	0.13	0.8
700	0.62	0.1	1	0.06	0.9

Table IV - 4 EIS fitting results for 50 vol% CuO-containing cell at different temperature

T[°C]	R_Ω [Ω cm^2]	R_1 [Ω cm^2]	n1	R_2 [Ω cm^2]	n2
600	1.13	0.41	0.8	0.53	1
650	0.74	0.13	0.9	0.09	1
700	0.43	0.05	0.9	0.02	1

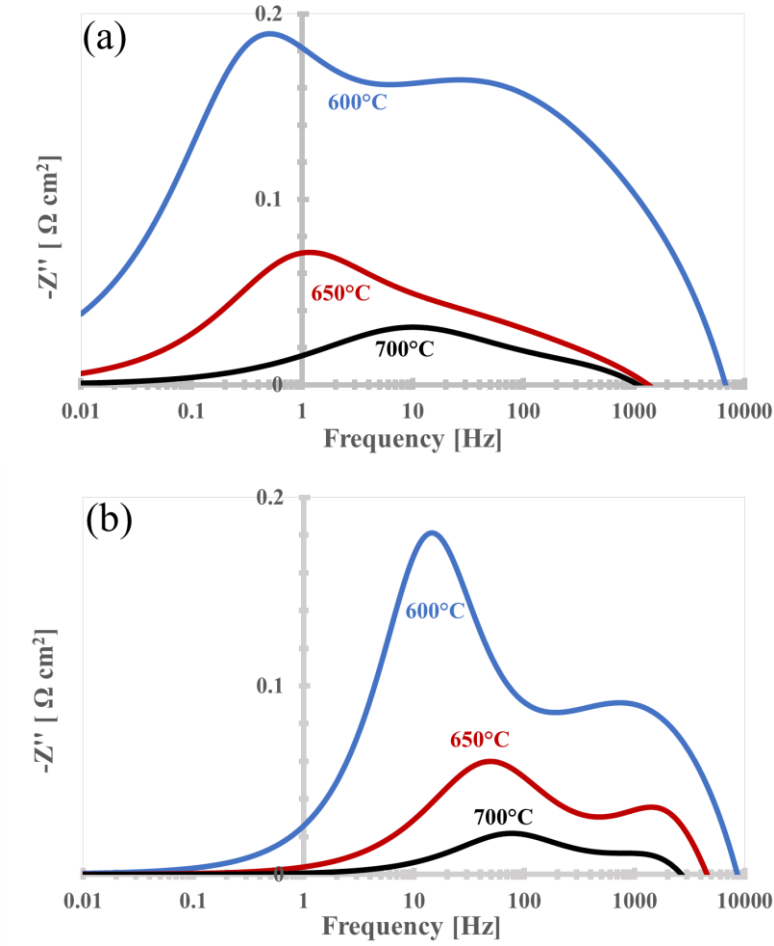

Figure IV – 31 Imaginary part of Bode plot for 45 vol% (a) and 50 vol% (b) CuO – containing cells at different temperature.

4.5.1.2 Effect of anode/electrolyte thickness ratio (r)

Planar anode-supported IT-SOFC were obtained after sintering at 900°C for thickness ratio (r) varying from 2 to 10.

Figure IV - 32 compares the electrolyte microstructure for 45 vol% CuO-containing cells with r = 2, 5 and 10.

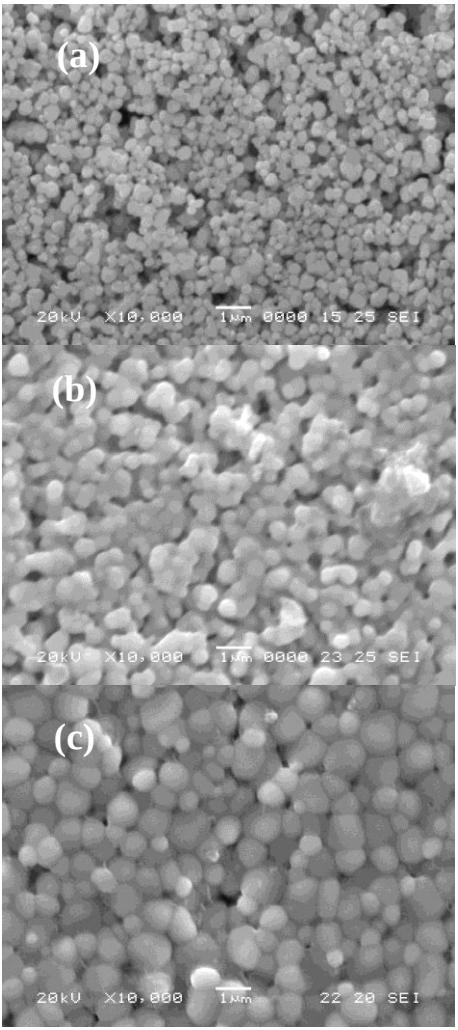

Figure IV - 32. Electrolyte surface in 45 vol% CuO containing cell with r=2 (a), r=5 (b) and r=10 (c).

The micrographs show a progressively advanced sintering level, thus confirming that, by increasing r (Eq. (1.1)), more intense compressive stress is generated upon sintering in the electrolyte layer. With $r = 2$, the GDC-based electrolyte is characterized by diffuse porosity and mostly isolated small particles (Fig. IV - 32(a)). The situation

improves when *r* = 5 (Fig. IV - 32(b)), while an almost fully densified / gas-tight electrolyte (Fig. IV - 32(c)) is obtained for anode/electrolyte thickness ratio r = 10.
The effect of a better electrolyte densification is confirmed by the polarization and power density curves shown in Figure IV - 33(a), where the electrochemical performance at 650°C of by 45 vol% CuO-containing cells realized with r = 5 and 10 is compared.

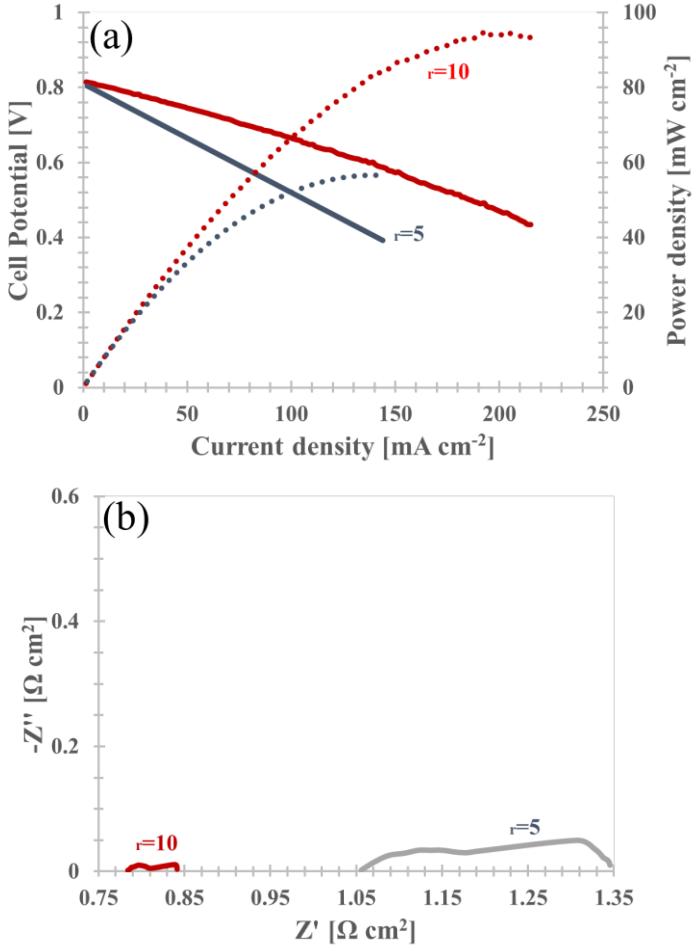

Figure IV - 33. Polarization and power density curves (a) and impedance spectra (b) of 45 vol% CuO containing cell at 650°C with r=5 and r =10.

Clearly, the cell with r =2 could not be electrochemically characterized because of the non-acceptable electrolyte microstructure. Interestingly, the power density peak

increases with the anode thickness, from ≈60 $mWcm^{-2}$ to 100 $mWcm^{-2}$ for *r* changing from 5 to 10. The electrolyte ohmic resistance (R_Ω) is usually associated with the first intersection with the real part axis in the Nyquist plot (Fig. IV - 33(b))[60]. As one can observe, R_Ω decreases when *r* is increased for 45 vol% CuO containing cell at 650°C (from ≈ 0.76 Ω cm^2 to ≈1.05 Ω cm^2 for r changing from 5 to 10), this being definitely accounted for by the better electrolyte densification. Such behaviour was recorded also during the tests carried out at the other temperatures and reported in Table IV - 5. As one can observe, for a given anode-to-electrolyte thickness ratio, R_Ω decreases by about one half for each 50°C, this being related to the improved GDC ionic conductivity. For a given temperature, both power density and ohmic resistance improve by ≈ 40% when r =10. According to this first set of results, it is clear that the most promising performances can be achieved by SOFC realized using an anode-to-electrolyte thickness ratio equal to 10; such architecture was therefore considered for the analysis of the CuO anode content.

Figure IV - 34 shows the electrolyte microstructure for the 50 vol% CuO-containing cell with r =10 which resembles the gas-tight electrolyte obtained using lower copper content (Fig. IV - 33(c)).

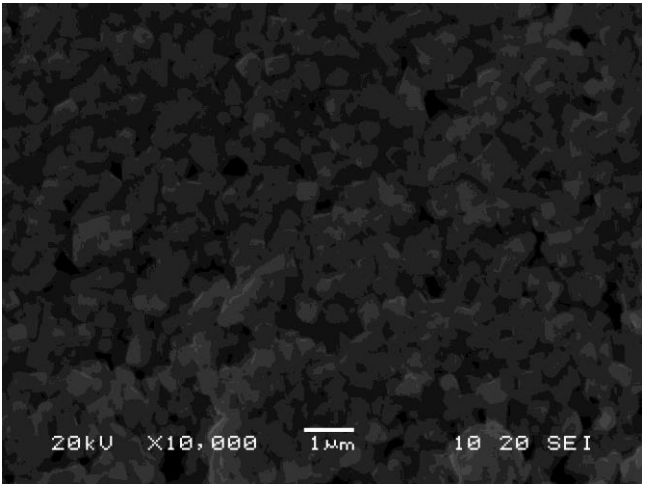

Figure IV - 34. Electrolyte surface in 50 vol% CuO containing cell with r=10

Therefore, a slightly larger CuO amount in the anode does not seem to influence the electrolyte sintering to a significant extent. The electrochemical performance of the corresponding IT-SOFC between 600°C and 700°C are shown in Fig. IV - 35.

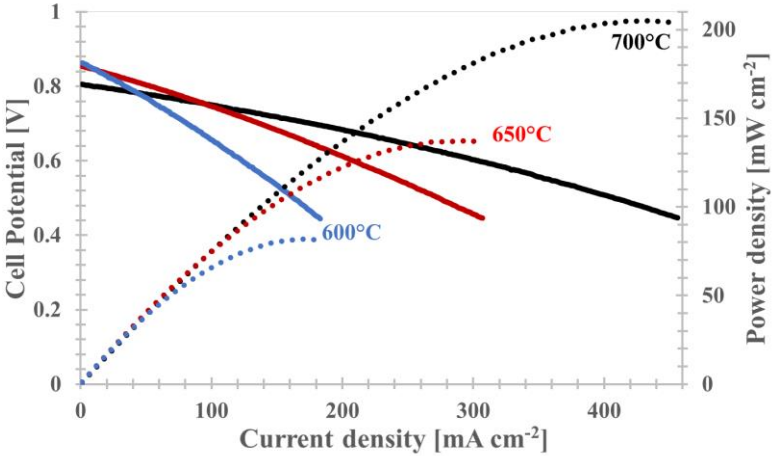

Figure IV - 35: Polarization and power density curves of 50 vol% CuO containing cell at different temperatures:

The cell reaches power density of 80, 150 and 200 mW cm^{-2} at 600 °C, 650 °C and 700°C, respectively. Very interestingly, the power density at 650°C is increased by a factor of six with respect to similar IT-SOFC whose anode contained 35 vol% CuO. Therefore, larger copper content within the CuO/GDC anodic cermet is confirmed to be certainly beneficial for the overall cell performance, because of the enhanced electrical conductivity. It is anyway important to remind that larger copper concentration could be introduced in the anode because the larger thickness of this latter allowed to reduce the sintering temperature to 900°C, thus limiting also the residual stresses during the cooling stage after sintering.

4.5.1.3 Effect of pore former addition

The addition of a certain amount of pore former within the anodic cermet affects the microstructure and the cell performance. Figure IV - 36 shows the electrochemical performance of the 50 vol% CuO containing cell with 5 wt% of pore former (i.e.: starch from rice) at different temperatures between 600°C and 700°C.

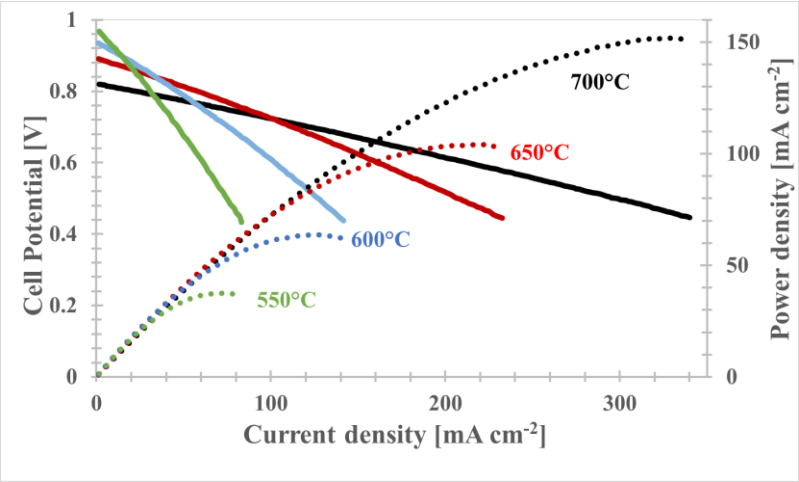

Figure IV - 36. Cell Potential and Power Density vs. Current Density of the 50 vol% CuO containing SOFC with 5 wt% pore former addition, at different temperatures.

In Figure IV – 37 one can observe the impedance spectra, while IV – 38 provides the Bode plots.

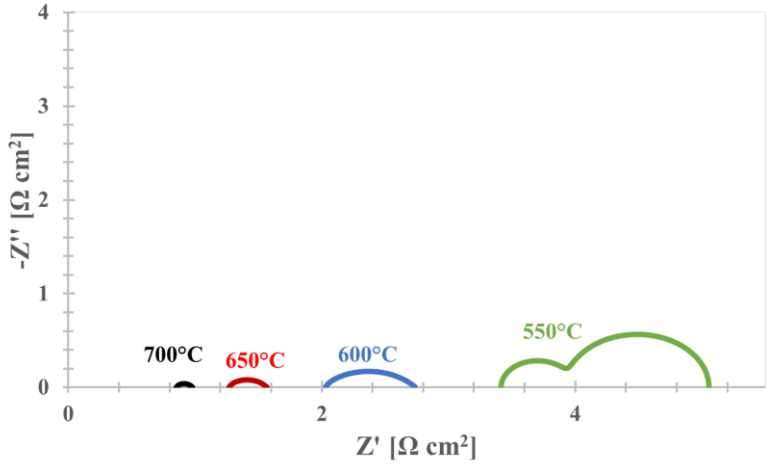

Figure IV - 37. Impedance spectra of the 50 vol% CuO containing SOFC with 5 wt% pore former addition, at different temperatures.

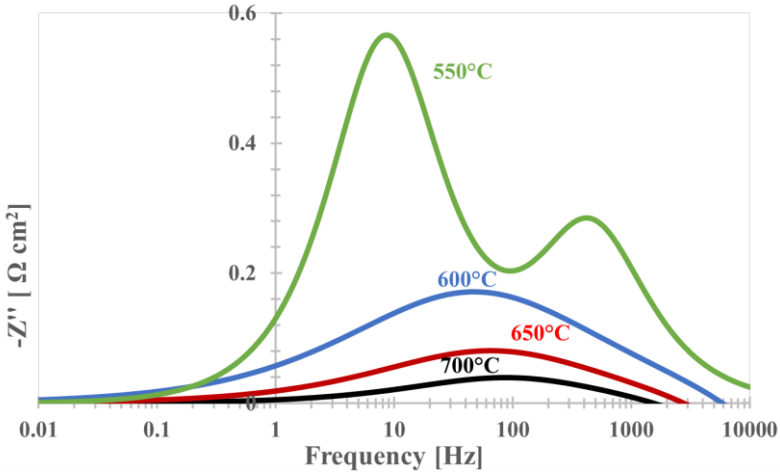

Figure IV - 38. Bode plot of the 50 vol% CuO containing SOFC with 5 wt% pore former addition, at different temperatures.

At 600°C, the cell achieves power density of ≈ 60 mW cm^{-2}. Power density increases with testing temperature reaching 150 mW cm^{-2} at 700 °C mA cm^{-2}. In particular, two distinguished effect can be analysed. Firstly, for all the operating temperatures, the pore former addition accounts for an OCV improvement, of 70, 40 and 20 mV at 600°C, 650°C and 700°C, respectively, compared with those obtained with the anode with no pore former. Conversely, the overall cell performance results reduced. Figure IV – 39 provides a comparison between performance achieved at 650°C with and without pore former.

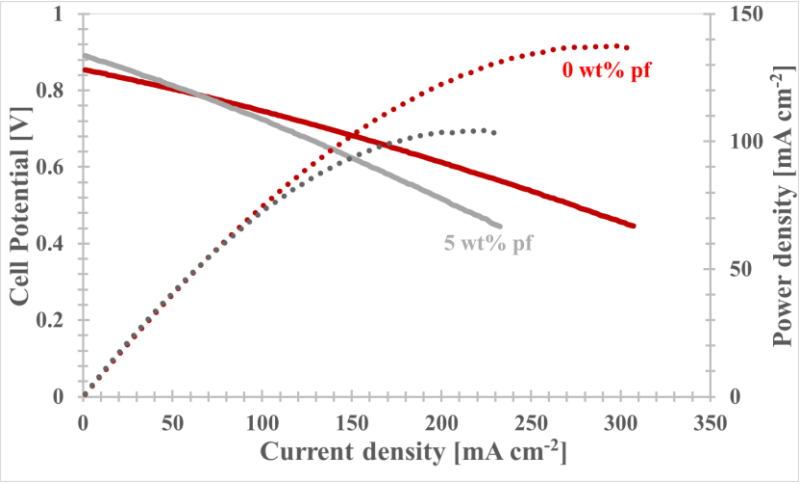

Figure IV - 39 Cell Potential and Power Density vs. Current Density of the 50 vol% CuO containing SOFC with and without 5 wt% pore former addition, at 650°C.

Although the improved OCV, the no pore former-containing cell achieves a power density ≈ 40% better (140 mW cm^{-2}).This is likely due to a less sintered electrolyte, resulting in an enhanced ohmic resistance (Fig IV – 40).

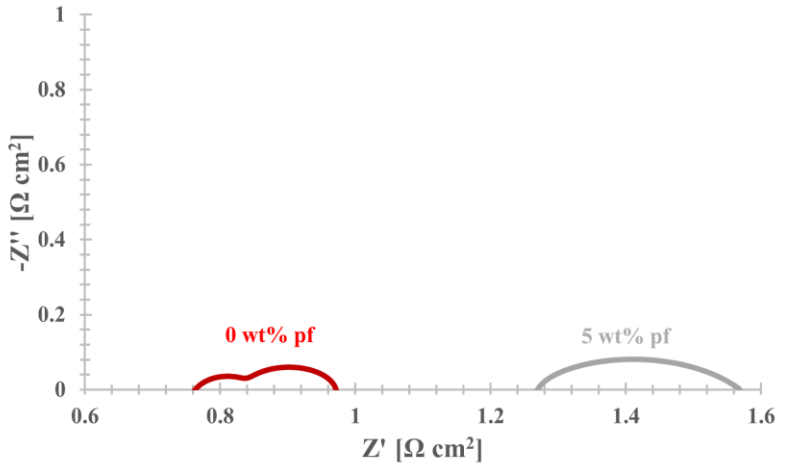

Figure IV – 40 Impedance spectra of the 50 vol% CuO containing SOFC with and without 5 wt% pore former addition, at 650°C.

According with Eq. 4.1, the pore former inhibits the anode sintering and, consequently, the reduced compressive stress on the electrolyte does not allow

obtaining a gas tight microstructure. Moreover, impedance spectra reveals a difference in the shape at varying frequencies. In fact, the pore former addition accounts for only one arc, with respect to the high and low frequency arcs commonly detected, as well as for no pore former-containing cell. Bode plots (Fig IV – 37) confirm such behaviour.

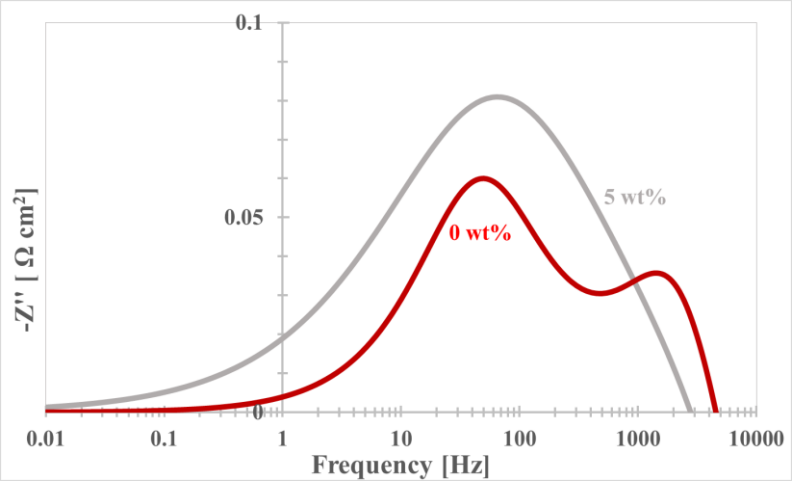

Figure IV – 41 Bode plot of the 50 vol% CuO containing SOFC with and without 5 wt% pore former addition, at 650°C.

SEM observations aid to integrate the analysis. As expected, the electrolyte reveals a more advanced stage of sintering when no pore former is employed, both in the cross section and in the fracture surface (Fig IV – 42 a, b, c, d). Moreover, the pore former addition accounts for a huge modification of anode microstructure (Fig IV – 42 e, f), this probably causing the different qualitative impedance behaviour[62]. Furthermore, EDS analysis revealed the presence of a certain amount of copper on the electrolyte surface of the pore former-containing SOFC, this suggesting the needs of a gas tight electrolyte microstructure for long operation work.

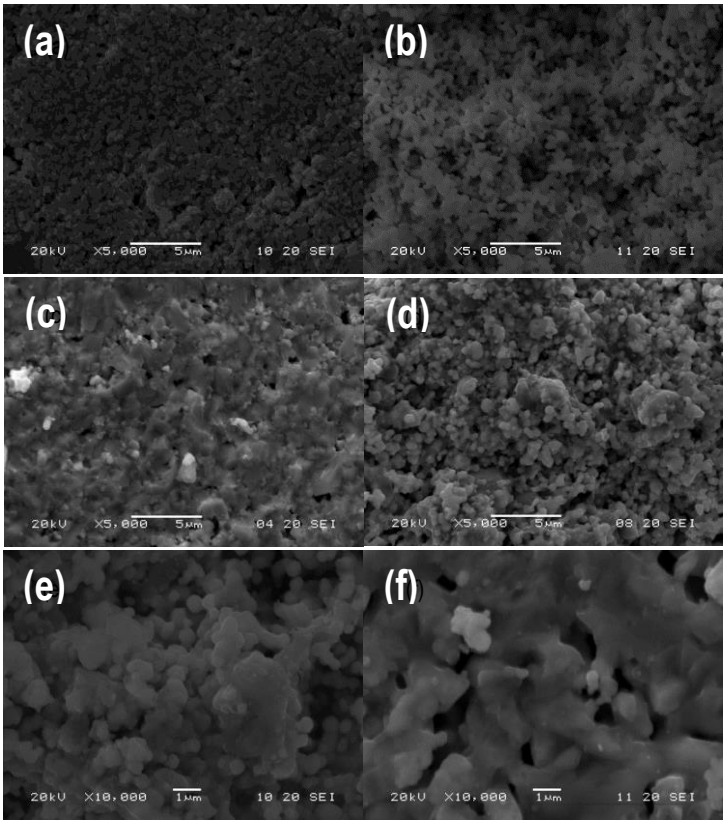

Figure IV – 42 Electrolyte cross surface of the 50 vol% CuO containing SOFC without (a) and with (b) 5 wt% pore former addition, at 650°C. Electrolyte fracture surface of the 50 vol% CuO containing SOFC without (c) and with (d) 5 wt% pore former addition, at 650°C. Anode cross surface of the 50 vol% CuO containing SOFC without (e) and with (f) 5 wt% pore former addition, at 650°C.

4.5.1.4 Effect of cell operation on the copper migration

Fig. IV – 43 shows the electrochemical performance at 600°C of 35vol% CuO containing cell sintered at 950°C (Cu35) and of 45 vol% CuO containing cell (Cu45) sintered at 900°C.

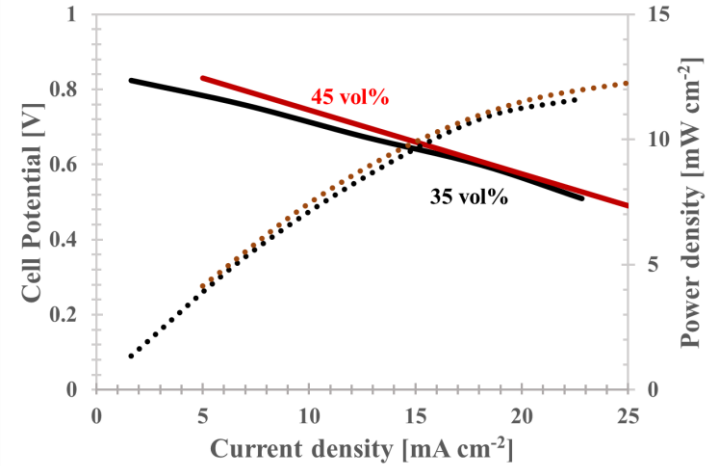

Figure IV – 43 Electrochemical performance of 35 and 45 vol% CuO containing SOFC at 600°C

Despite an higher OCV is expexted for Cu35, due to its better electrolyte densification, the OCV of Cu35 and Cu45 is 0.83 and 0.85, respectively. Such limited relative difference (less than 3%) is likely due to some aleatory (e.g.: concentrated losses in Cu35 or difference between the actual and the measured air flow in one or both tests). Both cells achieve power density of 12 mW cm^{-2} at current density ≈ 25 mA cm^{-2}. Similar polarization and power density curves were obtained for the cells containing different CuO load in the anode and sintered at different temperature. In order to distinguish the effect of such parameters Nyquist and Bode plots were recorded as shown in Fig. IV - 44.

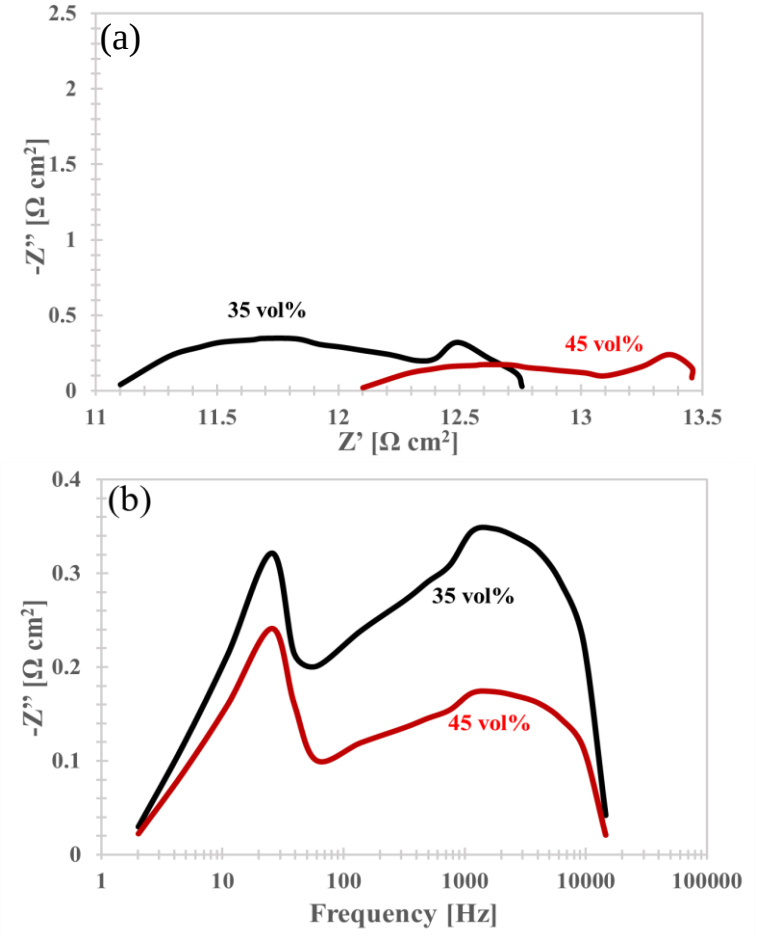

Figure IV – 44 Nyquist (a) and Bode (b) plot for 35 and 45 vol% CuO containing SOFC at 600°C.

Two arcs are clear in all spectra. In Nyquist plot (Fig. IV – 44(a)), the electrolyte ohmic resistance (R_Ω) is always associated with the first intersection of the curve with the real part axis[62] here occurring at about 11 Ω cm^2 and 12 Ω cm^2 for Cu35 and Cu45 cell, respectively. As previously reported[63], higher sintering temperature allows to reduce both bulk and grain boundary resistance and, on this basis, it is therefore possible to explain the lower electrolyte ohmic resistance of Cu35 cell. Therefore, regardless the Cu content in the anode, a more densified electrolyte structure accounts for larger ionic GDC conductivity. The estimated electrolyte ohmic resistance is here relatively

high, this being related to the fairly large thickness of the GDC membrane (equal to about 50 μm). It could be very likely reduced by using different electrolyte fabrication strategies, like, for example, screen printing[64, 65]. Figures Fig. IV - 45a and Fig. IV - 45b provide the electrolyte fracture surface of Cu35 and Cu45, respectively. The checked electrolyte thickness has was ≈55 μm for both cells.

The spectra in Fig. IV - 44 were analyzed according to the equivalent circuit in Fig. Fig. IV - 29, where R_1 and R_2 are the charge transfer resistance and mass transfer resistance, respectively.[62] R_1 depends on the hydrogen electro-oxidation and oxygen reduction reactions and it is associated with the high frequency arc in Fig. 5(b).[19] Conversely, R_2 depends on the gas-transport phenomena occurring at the anode and cathode sides and it is related to the low-frequency arc. [66, 67].

Fitting the plots in Fig. Fig. IV – 44 according to the equivalent circuit in Fig. Fig. IV - 29, the three resistances (R_Ω, R_1 and R_2) can be estimated as reported in Table IV - 6. In agreement with previous observation, R_Ω decreases of ≈ 10% from Cu35 to Cu45 cell, this pointing out a better electrolyte densification in the SOFC sintered at higher temperature. The impedance analysis reveals that, for this specific case, the electrolyte ohmic resistance is predominant (≈ 11-12 Ω cm^2) in comparison to the losses associated with the electrodes (less than 1 Ω cm^2). Therefore, the anode composition does not significantly affect the ohmic resistance, this being mainly due to the electrolyte[62, 68].

The polarization resistances, R_1 and R_2, decrease in Cu45. In particular, R_1 decrease with the Cu content, while R_2 decreases with lowering the sintering temperature, due to the increase in the porosity of anode. For 35 vol% CuO – containing anode, R_1 is equal to 1.1 Ω cm^2 and decreases down to 0.7 Ω cm^2 by increasing the Cu content. In the Cu-GDC anode formulation considered in the present work, using pure H_2 as anodic fuel, the catalytic activity towards H_2 oxidation reaction was ascribed to Cu^0, while ceria provides creation of oxygen vacancies[69].Therefore, despite 35 vol% CuO is enough to realize an operating electrode, larger CuO load is responsible for more efficient electrons mobility within the anode, this reducing the charge transfer phenomena[18]. One can therefore conclude that, regardless the sintering temperature, larger Cu load in the anode is responsible for lower charge transfer resistance. On the other hand, the mass transfer resistance appears independent on both sintering temperature and CuO concentration in the anode, the mass transfer phenomena being much more influenced by temperature variations, as previously reported.[66]

After the electrochemical characterization, some cells were manually but carefully broken to expose a fracture surface orthogonal to the cell plane. The microstructure was analyzed by Scanning Electron Microscopy (SEM) coupled with Energy Dispersive X-ray Spectroscopy (EDS). As shown in Fig. III – 1 (a and b), the produced fracture surfaces were divided into 9 different sections within the anode thickness, position 1 and 9 corresponding to the outer portion and the anode/electrolyte interface, respectively.

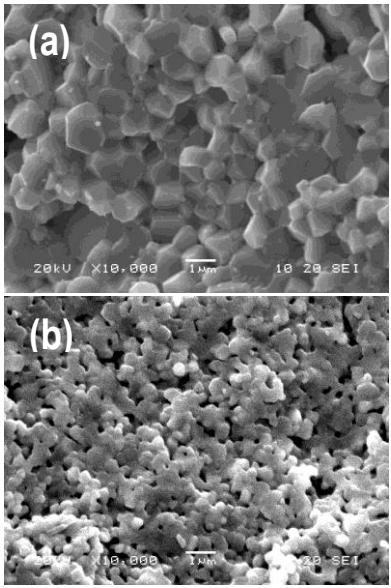

Figure IV – 45 Electrolyte fracture surface of 35 vol% (a) and 45 vol% CuO-containing anode (b) supported SOFC

Table IV – 6 Impedance spectra fitting parameters the two SOFC at 600°C

	R_Ω (Ω cm^2)	R_1 (Ω cm^2)	R_2 (Ω cm^2)
35 vol% CuO	12.3	1.1	0.6
45 vol% CuO	11.1	0.7	0.5

For each section, Cu and Ce content was evaluated and comparison was made between cells before and after the electrochemical characterization. Cu and Ce content was measured on SOFC fracture surface in correspon
dence of the anode as specified before. Table IV - 7 compares the results obtained on section 1 and 9, before and after the operation. In the former case, Cu concentration is substantially constant in the two considered sections; this demonstrates a homogeneous Cu distribution in the anode (≈32% and ≈40% for Cu35 and Cu45 cells, respectively).

Conversely, after cells operation, a relatively large difference in copper concentration between the considered sections can be pointed out, suggesting a certain diffusion within the anode during cell operation. For Cu35 anode, copper content decreases from 33% to 27% in section 1 after the operation, this corresponding to a relative difference of about 18%. The effect is even more evident in section 9 where Cu concentration increases from 31 to 44 wt%, corresponding to a relative increment of

≈ 42%. For Cu45 anode, the relative difference in section 1 and 9 is ≈-12.5 wt%, and ≈+15%, respectively. Figure Fig. IV - 47 summarizes the results collected by analysing all 9 sections in Fig. Fig. III - 1: here, Cu concentration is plotted as a function of the depth from the anode surface (100% depth corresponds to the electrolyte/anode interface). In both cases the migration of copper towards the electrolyte/anode interface is evident, this being responsible of Cu content reduction in the surface layers.

Table IV – 7 EDX quantitative analysis results for 35 and 45 vol% CuO containing anode before and after the reduction

Anode CuO content (vol%)	Copper concentration [wt%]			
	Before reduction		After reduction	
	Section 1	Section 9	Section 1	Section 9
35	33	31	27	44
45	40	39	35	45

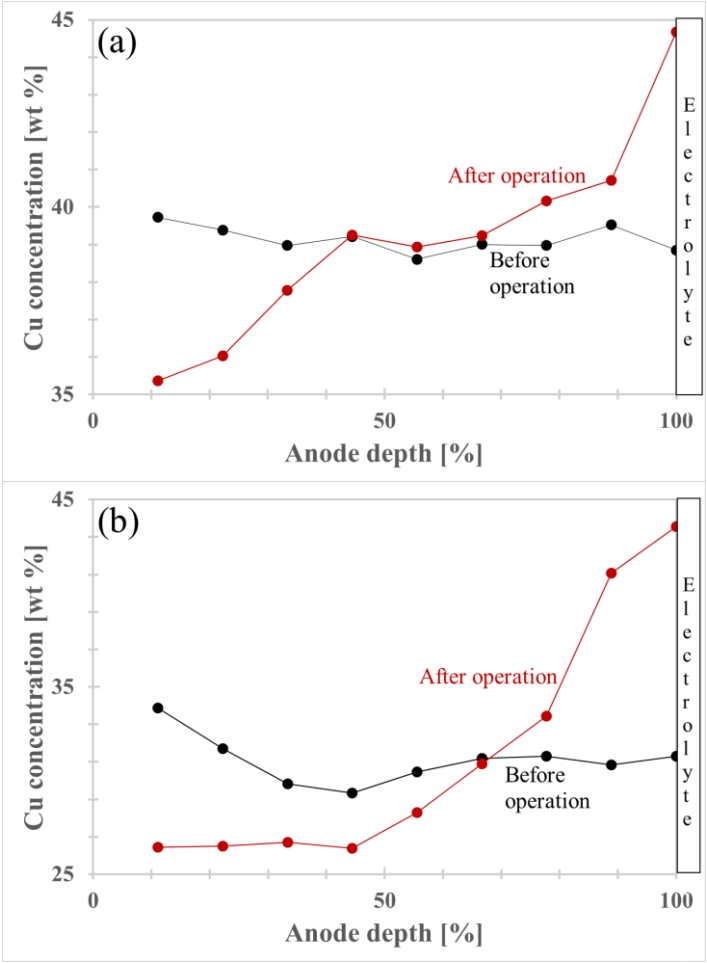

Figure IV – 47 Before- and after-operation Cu concentration for (a) 45 vol% and (b) 35 vol% CuO containing anode.

According to previous works, metallic atoms and/or ions can migrate in a metal/ceramic system due to grain boundary and surface diffusion phenomena[70]. It is reasonable to hypothesize the diffusion and the aggregation of copper in the Cu/GDC system, even at relatively low temperature (430°C), mainly because of concentration gradients between the anode and electrolyte, as observed in previous works on Ni/YSZ-based anodic layers[71, 72].

4.5.1.5 Effect of temperature

In order to clarify the role of the operating temperature on cell performance, 25 vol% CuO-containing cell was analysed in detail and the obtained results were compared with those obtained for the other cells. Starting from the polarization curves (Fig. IV – 21), according to previous well-defined theory, it is possible to distinguish among activation, ohmic and concentration overpotential contribution. In particular, the total resistance R(j) was considered as the key parameter, it being the average slope of the voltage-current density (V-j) curve. From an analytical point of view, R(j) can be described as:

$$R(j) = R_0 + \int \frac{dR}{dj} dj \qquad (4.3)$$

where R_0 is the first recorded resistance and $\int \frac{dR}{dj} dj$ the total variation of R between the starting point and the given j. For purely ohmic condition, $\int \frac{dR}{dj} dj = 0$ and $R(j) = R_0$, the V-j plot becoming perfectly linear.

In order to evaluate the different resistances contribution, R(j) - j plots were extrapolated from the polarization curves in Fig. IV - 21. According to Eq. (4.3), R_0 can be considered as:

$$R_0 = \frac{OCV - V_1}{j_1 - j_0} \qquad (4.4)$$

where V_1 is the second potential value following the OCV, j_1 the current density at V_1 and j_0 the current density at OCV (≈0). The integral in Eq. (4.3) can be approximated as

$$\therefore \frac{dR}{dj} dj \approx R_i - R_{i-1} \qquad (4.5)$$

where:

$$R_i = \frac{OCV - V_i}{j_i - j_0} \qquad (4.6)$$

the subscript i being referred to the i-th measurement. By plotting the calculated R(j) as a function of j, it is possible to distinguish the different overpotential contributions. R(j) vs j plot for 25 vol% CuO-containing cell between 600°C and 800°C, is shown in Fig. IV – 48.

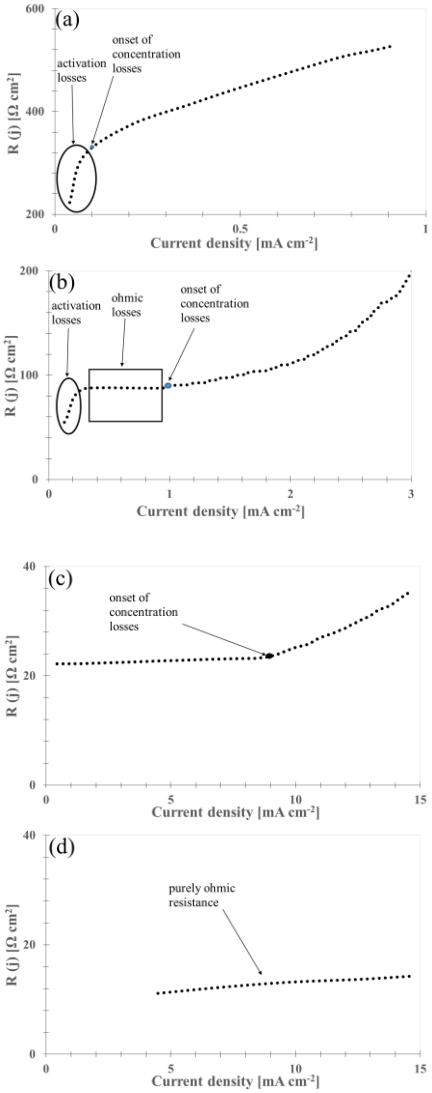

Figure IV – 48 Total impedance trend as a function of current density for 25 vol% CuO-containing cell at 600°C (a), 700°C (b) and 800°C (c) and for 35 vol% CuO-containing cell at 600°C (d).

A huge activation barrier (≈ 30 mV) can be identified at 600°C, probably due to the unfavorable kinetic at such relatively low temperature[74]. According to the literature[75-78], the activation overpotential corresponds to the first part of the polarization curve, at very limited current density. Therefore, a strong variation at the beginning of the R(j) - j plot is normally associated with activation losses. Figure IV – 46(a) also reveals the absence of a purely ohmic region. This can be very likely accounted for the limited diffusion coefficient at 600°C. For large current density, the limiting value (j_0) is reached, this generating the concentration overpotential. In fact, as a larger current is drawn from the cell, the reactions become faster and the reacting species begin to be depleted in one or both electrodes. When the limiting reaction step is completely dominated by the mass diffusion of the species towards and from the electrodes, the limiting current density j_0 is reached. This can be expressed as[79]:

$$j_0 = K D \qquad (4.7)$$

where K is a constant depending on the material, electrochemical reactions and thickness of the diffusion layer and D the mass diffusion coefficient. Therefore, for a given electrolyte, one can assume that the limiting current depends only on the diffusion coefficient. Approximately, it can be identified as the point where the behaviour of the cell deviates from linearity in the R (j)-j plot.

Therefore, at 600°C, the reactants at the anode side are affected by a limited diffusion, which reduces the limiting current below 0.08 mA cm^{-2}. When temperature is increased up to 700°C, the activation losses effect is reduced from ≈ 30 mV (Figure IV – 48(a)) to ≈10 mV (Figure IV – 48(b)). Moreover, the concentration losses onset is located at about 1 mA cm^{-2} more than ten times larger than at 600°C. Activation overpotential losses completely disappear if the cell operates at 800°C (Figure IV – 48(c)). The limiting current onset occurs at ≈ 8.5 mA cm^{-2} and it is about eight times larger than at 700°C. Therefore, the progressive favourable kinetic conditions at higher temperature allow to reduce the activation polarization. Figure IV – 48(d) shows the R(j) – j plot for 35 vol% CuO-containing cell at 600°C. As one can observe, 35 vol% CuO content is enough to completely overcome activation and concentration overpotential for the considered current densities, even at 600°C.

4.5.2 Cell tests in CH_4/CO_2 mixture

Figure IV - 49 shows the electrochemical performance of the 45vol% CuO-containing cell at 650°C and 700°C. At 650°C. As one can observe, the OCV is nearly constant at ≈ 0.6 V. Since the biogas composition is made only of 60 vol% of CH_4, the difference between experimental and theoretical OCV could be due related to such factor. The cell achieves power density of ≈ 26 mW cm^{-2} at current density of 120 mA cm^{-2}. Power density increases with testing temperature reaching 38 mW cm^{-2} at 140 mA cm^{-2}. As already underlined, the limited maximum power density is associated to the relatively large electrolyte thickness that is responsible ohmic resistance above 1

Ω cm^2 even at 700°C, as shown in figure IV – 50. Figure IV - 51 shows the Bode plot. As expected, there is a strong improvement of the mass diffusion process at 700°C, this being identified in the low-frequencies arc peak.

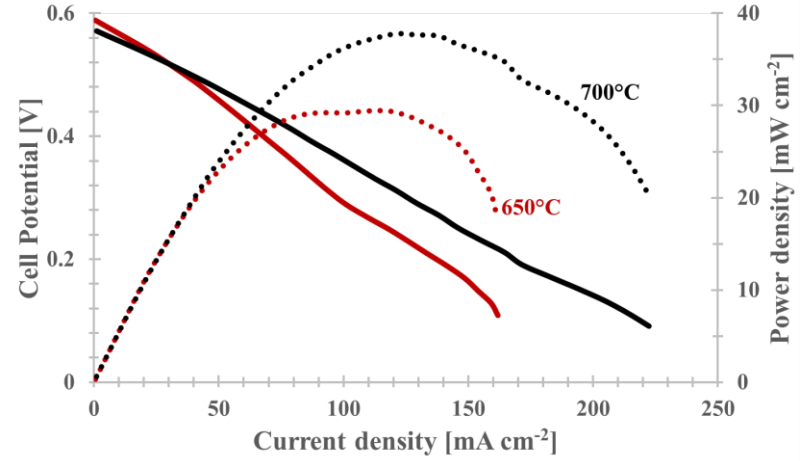

Figure IV – 49 Electrochemical performance of 45 vol% CuO containing SOFC in biogas at 650°C and 700°C

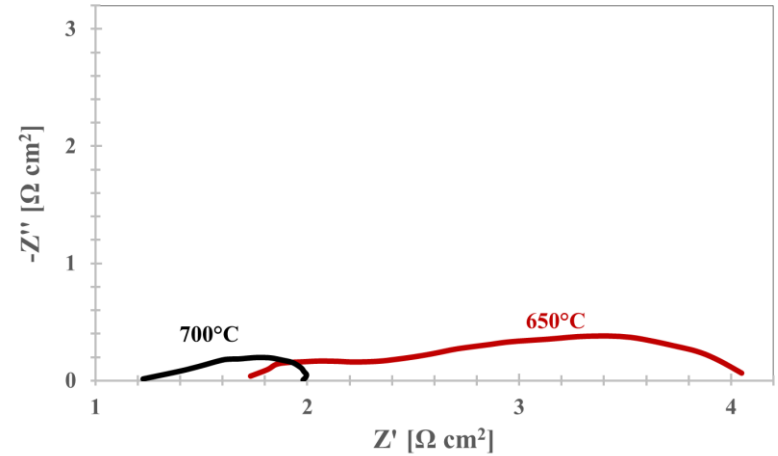

Figure IV – 50 Nyquist plot for 45 vol% CuO containing SOFC in biogas at 650°C and 700°C

In order to analyse such results, the cayalytic activity of CuO/GDC based cermet was studied. Regarding the dry reforming reaction, at the operating temperature of 700°C

there was no production of CO and H_2, this indicating the absence of catalytic activity for both the dry reforming reaction and for reaction that could lead to the production of carbon deposits, such as the methane decomposition:

$CH_4 = C + 2H_2$ (IV - 10)

Based on this first result, it is possible to state that there was no internal reforming within the anodes and this was due to the low Cu propension to the CH_4 reduction. The Cu-based cermet was also tested for the POM reaction, in order to better understand the catalytic role of Cu (Figure IV - 51). It is interesting to note that the molar ration between CH_4 and O_2 equal to 10 was chosen in order to unfavourite the combustion reaction $CH_4 + 2O_2 = CO_2 + 2H_2O$. Both the CH_4 e O_2 conversion increases at increasing the temperature. At 700 °C, the 97% of oxygen results converted, while CH_4 is limited to 5.6%, and the presence of CO and neither H_2 was revealed. Moreover, the POM reaction should lead to a methane conversion of 19%. Therefore, the reaction that takes place is the CH_4 combustion. Cu has no catalytic activity in methane reforming process (DRY o POM). Conversely, the GDC seems to catalyze the complete CH_4 combustion, even in low O_2 partial pressure conditions.

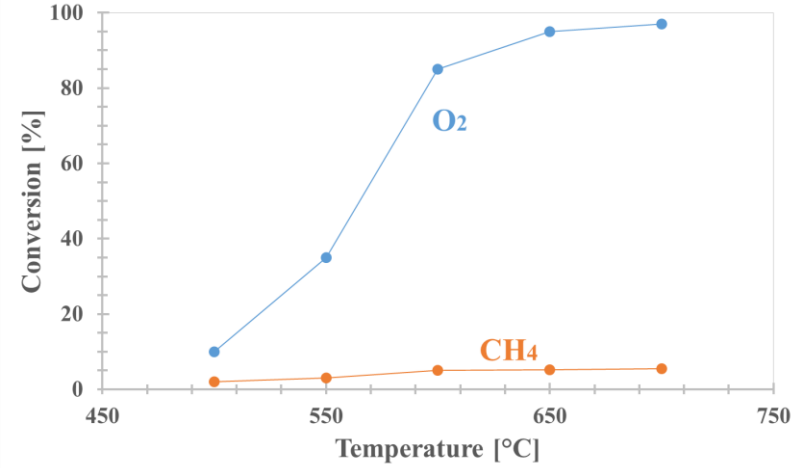

Figure IV – 51. Cataytic activity at different temperatures of CuO/GDC cermet for POM reaction.

Chapter V

Conclusions

5.1 Introduction

Planar Cu-based anode supported IT-SOFCs were produced in the present work. The copper was chosen as Ni-substitute for its reduced toxicity and high sulfur tolerance, this latter inhibiting the use of sulfur-containing fuels in Ni-based cells. Both anode and electrolyte were obtained by water-based tape casting, while the LSCF-based cathode was realized by screen printing.

5.2 IT-SOFC production

To obtain a defect free and smooth tape casting, the slurry recipe was optimized through analisys of viscosity, this providing a minimum shear stress value within the range of 0.1-0.3 mg m^{-2} of active part of dispersant. The effect of Bi_2O_3 and Li_2O as sintering aids for GDC were analysed by means of dilatometry and Archimede's method. Despite the enhanced sinterability, the bismuth oxide addition resulted not completely suitable for the aim of the present work. Conversely, it was possible to cosinter the cell at temperature lower than the CuO melting point (i.e. below 1100°C), by using 5 mol% Li_2O as sintering aid for GDC for the electrolyte and the anode, this latter inducing an advantageous compressive stress on the former upon sintering. In addition, due to the high thermal expansion mismatch, CuO load in the anode was equal to 35 vol%. Such cell was tested electrochemically between 550°C and 650°C and it reached a power density peak of 26 mW cm^{-2} at 650°C.

5.3 Improvement of IT-SOFC performance

In order to improve the cell performances, the anode/electrolyte thickness ratio was increased, this enhancing the compressive tensile stress on the electrolyte due to the constrained sintering process induced, so that a gas tight electrolyte was achieved at a reduced temperature. An advanced stage of sintering implies less ohmic resistance and, therefore, better performance for a given cell configuration. Moreover, it was shown that upon the cell operation, Cu could migrate towards the electrolyte/anode interface. Such phenomenon needs additional studies to understand whether it can influence the long-term performances of the cell. The reduced sintering temperature accounts for decreasing residual stress during the cooling stage of sintering. Thus, CuO content within the anodic cermet was enhanced up to 50 vol%. The realized cell revealed power density peak of ≈ 150 mW cm^{-2} at 650°C, this results meaning an improvement by a factor of 6 with respect to the 35 vol% CuO containing

IT-SOFCs sintered at 950°C, and of ≈ 200 mW cm^{-2} at 700°C. Moreover, EIS showed that 50 vol% CuO containing cermet provides performance comparable with conventional Ni-based anodic cermet.

5.4 Results in CH_4/CO_2 mixture

The 45 vol% CuO containing cell was tested electrochemically in biogas and reached a power density peak of ≈ 38 mW cm^{-2} at 700°C. The analysis of catalytic activity revealed that there is no methane reforming, while GDC catalyzes the complete CH_4 combustion, even in low oxygen partial pressure conditions. On this basis, the use of Cu/GDC based anodes represents a promising route to achieve the utilizations of sulfur-containing fuels for feeding IT-SOFC.

References [1-4]

[1] Minh, N.Q., Solid oxide fuel cell technology--features and applications, Solid State Ionics, 2004, 174: p.271-277.

[2] Doriya, M., Sofc systems and technology, Solid State Ionics, 2002, 152/153: p.383-392.

[3] Minh, N.Q., Ceramic fuel cells, Journal of American Ceramic Society, 1993, 76: p.563-588.

[4] Steele, B.C.H., Materials for fuel cells, Nature, 2001, 414: p.345-352.

[5] Wongchanapai, S., H. Iwai, M. Saito, and H. Yoshida, Performance evaluation of a direct-biogas solid oxide fuel cell-micro gas turbine (SOFC-MGT) hybrid combined heat and power (CHP) system, Journal of Power Sources, 2013, 23: p.1-17.

[6] Barelli, L., G. Bidini, F. Gallorini, and P. A. Ottaviano, Design Optimization of a SOFC based-CHP System through Dynamic Analysis, International Journal of Hydrogen Energy, 2013, 38: p.354-369.

[7] De Marco, V., G. Florio, and P., Fragiacomo, Optimal operation conditions for a methane fuelled SOFC and microturbine hybrid system, Journal of Renewable Energy, 2015, 15: 13 pages.

[6] Brett, D. J. L., A. Atkinson, N.P. Brandon, and S., Skinner, Intermediate Temperature Solid Oxide Fuel Cells, Chem. Soc. Rev., 2008, 37: p.1568-1578.

[7] Aguadero, A., L. Fawcett, S. Taub, R. Woolley, K. T. Wu, N. Xu, J. A. Kilner and S. J. Skinner, Materials development for intermediate- temperature solid oxide electrochemical devices, Journal of Material Science, 2012, 47: p.3925-3948.

[8] Inaba, H., and H. Tagawa, Ceria-based solid electrolyte, Solid State Ionics, 1996, 83: p. 1-16.

[9] Wright, H., T. Nakajima,and H. Tagawa, Sintering behaviors of ceria and gadolinia-doped ceria, Solid State Ionics 1998, 106: p.263-268.

[10] Esposito, V., M. Zunic, and E. Traversa, Improved Total Conductivity of Nanometric Samaria-Doped Ceria Powders Sintered with Molten $LiNO_3$ Additive, Solid State Ionics, 2009, 180: p.1069-1075.

[11] Mori, M., E. Suda, B. Pacaud, K. Murai and T. Moriga, Effect of Components in Electrodes on Sintering Characteristics of $Ce_{0.95}Gd_{0.1}O_{1.95}$ Electrolyte in Intermediate-Temperature Solid Oxide Fuel Cells During Fabrication, Journal of Power Sources, 2006, 157: p.688-694.

[12] Nicholas, J. D., and L. C. De Jonghe, Prediction and evaluation of sintering aids for Cerium Gadolinium Oxide, Solid State Ionics, 2007, 178: p.1187-1194.

[13] Accardo, G., C. Ferone, and R. Cioffi, Influence of Lithium on the Sintering Behavior and Electrical Properties of $Ce_{0.8}Gd_{0.2}O_{1.9}$ for Intermediate-Temperature Solid Oxide Fuel Cells, EnergyTechnology, 2016, 4: p.409-416.

[14] Gong, M., X. Liu, J. Trembly, and C. Johnson, Sulfur-tolerant anode materials for solid oxide fuel cell application, Journal of Power Sources, 2007, 168: p.289-298.
[15] Denkhaus, E., and K. Salnikov, Nickel essentiality, toxicity, and carcinogenicity, Critical Reviews in Oncology/Hematology, Critical Reviews in Oncology/Hematology, 2002, 42: p.35-36.
[16] Flytzani-Stephanopoulos, M., M. Sakbodin, and Z. Wang, Regenerative adsorption and removal of H_2S from hot fuel gas streams by rare earth oxides, Science, 2006, 312: p.508-510.
[17] Papurello, D., A. Lanzini, S. Fiorilli, F. Smeacetto, R. Singh and M. Santarelli, Sulfur poisoning in Ni-anode solid oxide fuel cells (SOFCs): Deactivation in single cells and stack, Chemical Engineering Journal, 2016, 283: p.1224-1233.
[18] He, H., R.J. Gorte, J.M. Vohs, Highly Sulphur tolerant Cu-Ceria Anodes for SOFCs, Electrochemical and Solid State Letters, 2005, 8: p. A279-A280.
[19] Bordia, R.K., and R. Raj, Sintering Behaviour of Ceramic Films Constrained by a Rigid Substrate, Journal of American Ceramic Society, 1985, 68: p. 287-292.
[20] Azzolini, A., V.M., Sglavo, and J.A. Downs, Fabrication and co-sintering of thin tubular IT-SOFC with Cu_2O-GDC cermet supporting anode and Li_2O-doped GDC electrolyte, Journal of European Ceramic Society, 2015, 35: p.2119-2127.
[21] Cologna, M., A.R. Contino, D. Montinaro, and V.M. Sglavo, Effect of Al and Ce doping on the deformation upon sintering in sequential tape cast layers for solid oxide fuel cells, Journal of Power Sources 2009, 5: p. 80-85.
[22] Cologna, M., A.R. Contino, V.M. Sglavo, S. Modena, S. Ceschini, M. Bertoldi, Curvature evolution and control in anode supported solid oxide fuel cells, Ceramic Engineering and Science Proceedings, 2009: p. 95.
[23] Cologna, M., V.M. Sglavo, and M., Bertoldi, Sintering and deformation of solid oxide fuel cells produced by sequential tape casting, International Journal of Applied Ceramic Technology 2010, 7, p. 803-813.
[24] Montinaro, D., V.M. Sglavo, M. Bertoldi, T. Zandonella, A. Aricò, M. Lo Faro, and V., Antonucci, Tape casting fabrication and co-sintering of solid oxide "half cells" with a cathode-electrolyte porous interface, Solid State Ionics 2006, 177, p. 2093-2097.
[25] Green, D.J., O. Guillon, J. Roedel, Constrained sintering: A delicate balance of scales, Journal of the European Ceramic Society, 2008, 28: p. 1451-1466.
[26] Green, D.J., P.Z. Cai, G.L. Messing, Residual Stresses in Alumina-Zirconia Laminates Journal of the European Ceramic Society, 1999, 19: p. 2511-2517
[27] Doe, U., Fuel Cell handbook, 2000, EG&G Services Inc..
[28] Singhal, S., High temperature solid oxide fuel cells: fundamental, design and applications, 2003.
[29] Subbarao, E., Solid electrolytes with oxygen ion conduction, Solid State ionics, 1984.
[30] Chen, Z., K. Ikeda, T. Murakami, and T. Takeda, Effect of particle packing on extrusion behavior of pastes. Journal of Material Science, 2000, 35: p. 5301-5307.

[31] Kaya, C., Extrusion of ceramic tubes with complex structures of non-uniform curvatures mades from nano-powders. Journal of the European Ceramic Society, 2004, 24: p. 3663-3670.
[32] Benbow, J., S. Jazayeri, and J. Bridgwater, The flow of pastes through dies of complicated geometry, Powder Technology, 1991.
[33] Khan, A. U., B. J. Briscoe, and P.F. Luckham, Evaluation of slip in capillary extrusion of ceramic pastes. Journal of the European Ceramic Society, 2001, 21: p. 483-491.
[34] Pabst, W., Fundamental considerations on suspension rheology, Ceramics silikaty, 2004, 48: p. 6-13.
[35] Reddy, J.J., M. Vijayakumar, T. Mohan, and P. Ramakrishnan, Loading of solids in a liquid medium: DETERMINATION of CVBC by torque rheometry.Journal of the European Ceramic Society, 1996, 16: p. 567-574.
[36] Atkinson, A., S.A. Baron, and N. P. Brandon, AC Impedance Spectra Arising from Mixed Ionic Electronic Solid Electrolytes, Journal of the Electrochemical Society, 2004, 151: p. E186-193.
[37] Ramesh, S. and CV Reddy, Electrical properties of co-doped $Ce_{0.8}$-x$Gd_{0.2}SrxO_{2-\delta}$ electrolyte, Acta Physica Polonica A, 2009, 115: p. 909-913.
[38] Nicholas J., and L. Delonghe, Prediction and evaluation of sintering aids for Cerium-Gadolinium Oxide, Solid state ionics, 2007, 178: p. 1187-1194.
[39] Kim, H., C. Lu, W. Worrell, J. Vohs, and R. Gorte, Cu-Ni cermet anodes for direct oxidation of methane in solid-oxide fuel cells. Journal of electrochemical Society, 2002, 149: p. A247-A250.
[40] Neumann, J., T. Zhong, and Y. Chang, The Cu-O (Copper Oxygen) system. Journal of Phase Equilibria, 1984, 5: p.136-140.
[41] Janardhanan, V.M., V. Heuveline, and O. Deutschmann, Performance analysis of a SOFC under direct internal reforming conditions. Journal of Power Sources, 2007, 172: p.296-307.
[42] Akbari-Fakhrabadi, A., R. V. Mangalaraja, F. A. Sanhueza, R. E. Avila, S. Ananthakumar, and S. H. Chan, Mechanical Properties of Gd-CeO_2 Electrolyte for SOFC Prepared by acqueous tape casting, Fuel Cells, 2013, 13: 682-688.
[43] Luo, L., A. Tok, and F. Boey, Aqueous tape casting of 10 mol%-Gd_2O_3-doped CeO_2 nano-particles, MATERIALS SCIENCE AND ENGINEERING A-STRUCTURAL MATERIALS PROPERTIES MICROSTRUCTURE AND PROCESSING 2006, 429: 266-271.
[44] Fu, Y.P., L. Yen-Chun, and H. Shao-Hua, Aqueous tape casting and crystallization behavior of gadolinium-doped ceria, Ceramics International, 2009, 35: 3153-3159.
[45] Mistler, R.E., and E.R., Twiname, Tape Casting – Theory and practice, Westerville: The American Ceramic Society, 2000.

[46] Akbari-Fakhrabadi, A., R. V. Mangalaraja, M. Jamshidijam, S. Ananthakumar, and S. H. Chan, Nanostructured Gd-CeO_2 electrolyte for solid oxide fuel cell by aqueous tape casting, Journal of Power Sources, 2012, 218: p.307-312.
[47] Phair, J., N. Lönnroth, M. Lundberg, and A. Kaiser, Characteristics of cerium-gadolinium oxide (CGO) suspensions as a function of dispersant and powder properties, Physicochem. Eng. Aspects, 2009, 341: p.103-109
[48] Azzolini, A., V.M. Sglavo, and J.A. Downs, Production and performance of Copper based Anode Supported SOFC, ECS Transactions, 2015, 68 issue 1: p.2583-2596.
[49] Cai, P.Z., D.J. Green, and G.L. Messing, Constrained densification of alumina/zirconia hybrid laminates, II: viscoelastic stress computation, Journal of American Ceramic Society, 1997, 80: p.1940-1948.
[50] Ho, S., C. Hillman, S. Lange and Z. Suo, Surface cracking in layers under biaxial, residual compressive stress, Journal of American Ceramic Society, 1995, 78: p.2353-235

9.
[51] Sglavo V.M., and M., Bertoldi, Design and production of ceramic laminates with high mechanical resistance and reliability, Acta Materialia 2006, 54: p. 4929-2937.
[52] Rao, M.P., J. Rödel, and F. F., Lange, Residual Stress Induced R-Curves in Laminar Ceramics That Exhibit a Threshold Strength, Journal of American Ceramic Society, 2001, 84: p. 2722-2724.
[53] Z. Chlup, H. Hadraba, D. Drdlik, K. Maca, I. Dlouhy, and R. Bermejo, On the determination of the stress-free temperature for alumina-zirconia multilayer structures, Ceram. Internat. 2014, 40: p. 5787-5793
[54] Reddy, L.H., G.K. Reddy, D. Devaiah, and B.M. Reddy, A rapid microwave-assisted solution combustion synthesis of CuO promoted CeO_2–$M_x O_y$ (M=Zr, La, Pr and Sm) catalysts for CO oxidation, Catalysis A: General, 2012, 445-446: p.297-305
[55] Boukha, Z., J.L. Ayastuy, A. Iglesias-González, B. Pereda-Ayo, M.A. Gutiérrez-Ortiz, and J.R. González-Velasco, Preparation and characterisation of CuO/Al_2O_3 films deposited onto stainless steel microgrids for CO oxidation, Applied Catalysis B: Environmental, 2014, 160-161: p.629-640.
[56] Aneggi, E., D. Wiater, C. de Leitenburg, J. Llorca, A. Trovarelli, Shape-dependent activity of ceria in soot combustion, ACS Catalysis, 2014, 4: p.172-181.
[57] Jiang, D., W. Wang, L. Zhang, Y. Zheng, Z. Wang, Insights into the Surface-Defect Dependence of Photoreactivity over CeO_2 Nanocrystals with Well-Defined Crystal Facets, ACS Catalysis, 2015, 5: p.4851-4858.
[58] Jung, H.Y., S.-H. Choi, H. Kim, J.-W. Son, J. Kim, H.-W. Lee, and J.-H. Lee, Fabrication and performance evaluation of 3-cell SOFC stack based on planar 10 cm × 10 cm anode-supported cells, Journal of Power Sources, 2006, 159: p.478-483.
[59] Jacques-Bédarda, X., T.W. Napporna, R. Robergeb, and M. Meuniera, Performance and ageing of an anode-supported SOFC operated in single-chamber conditions, Journal of Power Sources, 2006, 153: p.108-113.

[60] Huang, Q., R. Hui, B. Wang, J. Zhang, A review of AC impedance modeling and validation in SOFC diagnosis, Electrochimica Acta,2011, 52: p. 8144-8164
[61] Han, M., Z. Liu, S. Zhou, and L. Yu, Influence of Lithium Oxide Addition on the Sintering Behavior and Electrical Conductivity of Gadolinia Doped Ceria, Journal of Materials Science & Technology 2011, 27: p.460-464
[62] Brown, M., S. Primdahl, M. Mogensen, Structure/Performance Relations for Ni/Yttria-Stabilized Zirconia Anodes for Solid Oxide Fuel Cells, Journal of The Electrochemical Society, 2000, 147(2): p.475-485.
[63] Zheng, Y., C. Chen, S. Li, L. Ge, H. Chen, L. Guo, Effect of the sintering temperature on the properties of $Ce_{0.85}La_{0.10}Ca_{0.05}O_{2-\delta}$ electrolyte material, Materials Research Bulletin, 2011, 46: p.130-135.
[64] Zhao, L., X. Huang, R. Zhu, Z. Lu, W. Sun, Y. Zhang, X. Ge, Z. Liu, and W. Su, Optimization on technical parameters for fabrication of SDC film by screen-printing used as electrolyte in IT-SOFC, Journal of Physics and Chemistry of Solids, 2008, 69: p.2019-2024.
[65] Ried, P., C. Lorenz, A. Brönstrup, T. Graule, N. H. Menzler, W. Sitte, and P. Holtappels, Processing of YSZ screen printing pastes and the characterization of the electrolyte layers for anode supported SOFC, Journal of the European Ceramic Society, 2008, 28: p.1801-1808.
[66] Fu, C., S.H. Chan, Q. Liu, X. Ge, and G. Pasciak, Fabrication and evaluation of Ni-GDC composite anode prepared by aqueous-based tape casting method for low-temperature solid oxide fuel cell, International Journal of Hydrogen Energy, 2010, 35: p.301-307.
[67] Montinaro, D., A.R. Contino, A. Dellai, and M. Rolland, Determination of the impedance contributions in anode supported solid oxide fuel cells with $(La,Sr)(Co,Fe)O_{3-d}$ cathode, International Journal of Hydrogen Energy, 2014, 39: p.21638-21646.
[68] Barfoda, R., M. Mogensen, T. Klemensø, A. Hagen, Y.L. Liu and P.V., Hendriksen, Detailed Characterization of Anode-Supported SOFCs by Impedance Spectroscopy, Journal of the Electrochemical Society, 2007, 154: p.B371-B378.
[69] Lee, H. C., and D. H. Kim, Kinetics of CO and H_2 oxidation over $CuO\text{-}CeO_2$ catalyst in H_2 mixtures with CO_2 and H_2O, Catalysis Today, 2008, 132: p.109-116.
[70] Liu, Y.L., and C. Jiao, Microstructure degradation of an anode/electrolyte interface in SOFC studied by transmission electron microscopy, Solid State Ionics, 2005, 176: p.435-442.
[71] Chen, J.G., M.L. Colaianni, W.H. Weinberg, J.T. Yates, The $Cu/Al_2O_3/Al$ (111) interface: initial film growth and thermally induced diffusion of copper into the bulk Surface Science, 1992, 272: p.223-232.
[72] Aaberg, R.J., R. Tunold, M. Mogensen, R. W. Berg, and R. Ødegaård, Morphological Changes at the Interface of the Nickel-Yttria Stabilized Zirconia Point Electrode, Journal of The Electrochemical Society, 1998, 145: p.2244-2252.

[73] Ramesh, S., C. Vishnuvardhan Reddy, Electrical properties of co-doped ceria electrolyte $Ce_{0.8-x}Gd_{0.20}SrxO_{2-\delta}$, ACTA PHYSICA POLONICA A, 2009, 115: p.909-913.
[74] Mizusak, J., and H. Tagawa, Kinetics of the electrode reaction at the H_2-H_2O porous Pt/Stabilized zirconia interface, Journal of The Electrochemical Society: 1994, 141: p.1674-1683.
[75] Chan, S.H., K.A. Khor, and Z.T. Xia, A complete polarization model of a solid oxide fuel cell and its sensitivity to the change of cell component thickness, Journal of Power Sources, 2001, 93: p.130-140.
[76] Virkar, A.V., J. Chen, C.W. Tanner, and J.W. Kim, The role of electrode microstructure on activation and concentration polarizations in solid oxide fuel cells, Solid State Ionics, 2000, 131: p.189-198.
[77] Chan, S.H., H.K. Ho, and Y. Tian, Multi-level modeling of SOFC–gas turbine hybrid system, International Journal of Hydrogen Energy, 2003, 28: p.889-900.
[78] Ni, M., and M.K.H. Leung, Parametric study of solid oxide steam electrolyzer for hydrogen production, International Journal of Hydrogen Energy, 2007, 32: p.2305-2313.
[79] Qi, Y., B. Huang, and K.T. Chuang, Dynamic modeling of solid oxide fuel cell: The effect of diffusion and inherent impedance, Journal of Power Sources, 2005, 150: p.32-47.
[80] Conway, B.E., J.O.M. Bockris, and R.E. White, New York: plenum publishers Modern aspects of electrochemistry, New York, 1999, 32: p.143.
[81] Jiang, S.P., A review of wet impregnation-alternative method for the fabrication of high performance and nano-structured electrodes of solid oxide fuel cells, Materials science and engineering A, 2006, 418: p.199-210.
[82] Sun, H., Y. Chen, F. Chen, Y. Zhang, and M. Liu, High-performance solid oxide fuel cells based on a thin $La_{0.8}Sr_{0.2}Ga_{0.8}Mg_{0.2}O_{3-\delta}$ electrolyte membrane supported by a nickel based anode of unique architecture, Journal of Power Sources, 2016, 301: p.199-203.
[83] López-Robledo, M.J., M.A. Laguna-Berceroa, J. Silva, V.M. Orera, and A., Larrea, Electrochemical performance of intermediate temperature micro-tubular solid oxide fuel cells using porous ceria barrier layers, Ceramics International: 2015, 41: p.7651-7660.

Scientific production

ECS Transaction,

"Effect of Bismuth Oxide as Sintering Aid for Gadolinia-doped Ceria at 1050°C",
Volume 68, issue 1 (2015), 413-420

Ceramic Engineering and Science Proceeding,

"Production and co-sintering at 950°C of planar half-cells with CuO-GDC cermet supporting anode and Li_2O-doped GDC electrolyte",
Volume 37, Issue 3 (2016), 31-38, The American Ceramic Society

Journal of Power Sources

"Production of planar copper-based anode supported intermediate temperature solid oxide fuel cells cosintered at 950°C"
Volume 328, pp. 235-240, 2016.

Journal of the Ceramic Society of Japan

"Performance and evolution of planar copper-based anode-supported solid oxide fuel cells"
Volume 125 [4] 313-316 2017

International Journal of Hydrogen Energy

"Effect of anode thickness and Cu content on consolidation and performance of planar copper-based anode-supported SOFC"
To be published doi: 10.1016/j.ijhydene.2017.03.221

Fuel Cells

"Influence of copper-based anode composition on intermediate temperature solid oxide fuel cells performance"
To be published

Participation to Congresses, Schools and Workshops

Advances in Medium and High Temperature Solid Oxide Fuel Cells Technology. Udine, July 14th-18th 2014

International Workshop "Ceramics for Energy", Istec and Dipartimento di Chimica Industriale "Toso Montanari" of Alma Mater Studiorum of Bologna, Faenza (Ravenna), Italy , 14-15th May 2015

Poster Presentation "Production of GDC dense electrolyte by Water-based tape casting"

Workshop Electron Matter Interactions. Trento, 16th June 2015

ECS conference on Electrochemical Energy Conversion & Storage with SOFC XIV, Electrochemical Society, Glasgow, United Kingdom , 26-31st July 2015

Poster Presentation "Effect of Bismuth oxide as Sintering Aid for Gadolinia-doped Ceria at 1050°C"

40th International Conference of American Ceramic Society, American Ceramic Society, Daytona Beach, USA, 24-29th January 2016

Poster Presentation "Production and co-sintering at 950°C of Planar half-cells with CuO-GDC Cermet supporting anode and Li_2O-doped GDC electrolyte"

ECERS 2015 in Toledo, Spain, 21-26th June 2015;

"Effect of Bismuth Oxide as Sintering Aid for Gadolinia-Doped Ceria at 1050°C" (not personally present)

"Production of Li-doped GDC dense electrolyte at 950°C by water-based tape casting"

Poster presentation and Extended abstract published EFC2015 in Naples, 16-18th December 2015 (not personally present).

Other activities

2014/2015:

Lab activities of the course “Ceramic Materials Engineering”, Analysis of viscosity for production of Alumina Crucibles by slip casting;

Production of Zirconia Samples by water-based tape casting;

Production of Alumina Samples by water-based tape casting.

120h as tutor of Mathematics (60h in DICAM department and 60 h Economy Department)

2015/2016:

Lab activities of the course “Ceramic Materials Engineering”, Analysis of viscosity for production of Zirconia Crucibles by slip casting;

Production of Zirconia Samples by water-based tape casting;

Poduction of Alumina Samples by water-based tape casting.

100h as tutor of Mathematics (at the Economy Department)

100h as tutor of Statistics (50 at the Economy Department, 50 at Cibio)

2016/2017:

Lab activities of the course “Ceramic Materials Engineering”

Production of Zirconia Samples by water-based tape casting;

Analysis of viscosity for production of Alumina Crucibles by slip casting;

100h as tutor of Mathematics (Department of Industrial Engineering)

Master Thesis Co-Supervisor: “Production of High Performance Planar Copper-Based Anode-Supported IT-SOFCs” Saqib Rashid.